EUROPEAN ORGANIZATION FOR NUCLEAR RESEARCH

CERN–PPE/92-60

April 15, 1992

A Study of the Decays of Tau Leptons Produced on the Z Resonance at LEP.

DELPHI Collaboration

This paper is dedicated to the memory of Rafael Llosa.

Abstract

From the analysis of a data sample corresponding to an integrated luminosity of 4.63 pb^{-1} taken during the 1990 run of LEP at centre of mass energies between 88.2 GeV and 94.2 GeV, the tau decays $\tau^- \to e^-\bar{\nu}_e\nu_\tau$, $\tau^- \to \mu^-\bar{\nu}_\mu\nu_\tau$, $\tau^- \to \pi^-(K^-)\nu_\tau$, $\tau^- \to \rho^-\nu_\tau$ and their charge conjugates have been studied. The following branching ratios have been measured; $BR(\tau^- \to e^-\bar{\nu}_e\nu_\tau) = 18.6 \pm 0.8(stat) \pm 0.6(sys)\%$, $BR(\tau^- \to \mu^-\bar{\nu}_\mu\nu_\tau) = 17.4 \pm 0.7 \pm 0.6\%$, $BR(\tau^- \to \pi^-(K^-)\nu_\tau) = 11.9 \pm 0.7 \pm 0.7\%$, $BR(\tau^- \to \rho^-\nu_\tau) = 22.4 \pm 0.8 \pm 1.3\%$, in good agreement with world averages. The measured electronic and muonic branching ratios lead to a measurement of the strong coupling constant, $\alpha_s(m_\tau) = 0.26^{+0.09}_{-0.12}$. Extrapolating the α_s value from m_τ to m_Z yields $\alpha_s(m_Z) = 0.109^{+0.012}_{-0.028}$.

The average polarization P_τ of taus produced in $Z \to \tau^+\tau^-$ decays has also been measured using the above decay modes. The weighted mean of the polarizations obtained from the four decay modes is $P_\tau = -0.24 \pm 0.07$. This value of P_τ gives, in the improved Born approximation, a ratio between the axial and vector coupling constants of the tau of $v_\tau/a_\tau = 0.12 \pm 0.04$, and hence a value of the effective electroweak mixing parameter $\sin^2\theta_W(m_Z^2) = 0.220 \pm 0.009$.

(Submitted to Zeits. f. Phys. C)

P.Abreu[19], W.Adam[45], F.Adami[36], T.Adye[34], E.Agasi[28], G.D.Alekseev[13], P.Allen[44], S.Almehed[22], S.J.Alvsvaag[4], U.Amaldi[7], E.G.Anassontzis[3], A.Andreazza[26], P.Antilogus[23], W-D.Apel[14], R.J.Apsimon[34], B.Åsman[40], J-E.Augustin[17], A.Augustinus[28], P.Baillon[7], P.Bambade[17], F.Barao[19], R.Barate[11], G.Barbiellini[42], D.Y.Bardin[13], A.Baroncelli[37], O.Barring[22], J.A.Barrio[24], W.Bartl[45], M.J.Bates[31], M.Battaglia[26], M.Baubillier[21], K-H.Becks[47], C.J.Beeston[31], M.Begalli[33], P.Beilliere[6], Yu.Belokopytov[39], P.Beltran[9], D.Benedic[8], M.Berggren[17], D.Bertrand[2], F.Bianchi[41], M.S.Bilenky[13], P.Billoir[21], J.Bjarne[22], D.Bloch[8], S.Blyth[31], V.Bocci[35], P.N.Bogolubov[13], T.Bolognese[36], M.Bonesini[26], W.Bonivento[26], P.S.L.Booth[20], P.Borgeaud[36], G.Borisov[39], H.Borner[7], C.Bosio[37], B.Bostjancic[7], O.Botner[43], B.Bouquet[17], C.Bourdarios[17], T.J.V.Bowcock[20], M.Bozzo[10], S.Braibant[2], P.Branchini[37], K.D.Brand[32], R.A.Brenner[7], H.Briand[21], C.Bricman[2], R.C.A.Brown[7], N.Brummer[28], J-M.Brunet[6], L.Bugge[30], T.Buran[30], H.Burmeister[7], J.A.M.A.Buytaert[2], M.Caccia[7], M.Calvi[26], A.J.Camacho Rozas[38], T.Camporesi[7], V.Canale[35], F.Cao[2], F.Carena[7], L.Carroll[20], C.Caso[10], E.Castelli[42], M.V.Castillo Gimenez[44], A.Cattai[7], F.R.Cavallo[5], L.Cerrito[35], V.Chabaud[7], A.Chan[1], Ph.Charpentier[7], L.Chaussard[17], J.Chauveau[21], P.Checchia[32], G.A.Chelkov[13], L.Chevalier[36], P.Chliapnikov[39], V.Chorowicz[21], J.T.Chrin[44], R.Cirio[41], M.P.Clara[41], P.Collins[31], J.L.Contreras[24], R.Contri[10], E.Cortina[44], G.Cosme[17], F.Couchot[17], H.B.Crawley[1], D.Crennell[34], G.Crosetti[10], M.Crozon[6], J.Cuevas Maestro[38], S.Czellar[12], S.Dagoret[17], E.Dahl-Jensen[27], B.Dalmagne[17], M.Dam[30], G.Damgaard[27], G.Darbo[10], E.Daubie[2], A.Daum[14], P.D.Dauncey[31], M.Davenport[7], P.David[21], W.Da Silva[21], C.Defoix[6], D.Delikaris[7], B.A.Della Riccia[41], S.Delorme[7], P.Delpierre[6], N.Demaria[41], A.De Angelis[42], M.De Beer[36], H.De Boeck[2], W.De Boer[14], C.De Clercq[2], M.D.M.De Fez Laso[44], N.De Groot[28], C.De La Vaissiere[21], B.De Lotto[42], A.De Min[26], H.Dijkstra[7], L.Di Ciaccio[35], F.Djama[8], J.Dolbeau[6], M.Donszelmann[7], K.Doroba[46], M.Dracos[7], J.Drees[47], M.Dris[29], Y.Dufour[6], L-O.Eek[43], P.A.-M.Eerola[7], R.Ehret[14], T.Ekelof[43], G.Ekspong[40], A.Elliot Peisert[32], J-P.Engel[8], D.Fassouliotis[29], M.Feindt[7], A.Fenyuk[39], M.Fernandez Alonso[38], A.Ferrer[44], T.A.Filippas[29], A.Firestone[1], H.Foeth[7], E.Fokitis[29], F.Fontanelli[10], K.A.J.Forbes[20], B.Franek[34], P.Frenkiel[6], D.C.Fries[14], A.G.Frodesen[4], R.Fruhwirth[45], F.Fulda-Quenzer[17], K.Furnival[20], H.Furstenau[14], J.Fuster[7], G.Galeazzi[32], D.Gamba[41], C.Garcia[44], J.Garcia[38], C.Gaspar[7], U.Gasparini[32], Ph.Gavillet[7], E.N.Gazis[29], J-P.Gerber[8], P.Giacomelli[7], R.Gokieli[46], V.M.Golovatyuk[13], J.J.Gomez Y Cadenas[7], A.Goobar[40], G.Gopal[34], M.Gorski[46], V.Gracco[10], A.Grant[7], F.Grard[2], E.Graziani[37], G.Grosdidier[17], E.Gross[7], P.Grosse-Wiesmann[7], B.Grossetete[21], S.Gumenyuk[39], J.Guy[34], U.Haedinger[14], F.Hahn[7], M.Hahn[14], S.Haider[28], Z.Hajduk[15], A.Hakansson[22], A.Hallgren[43], K.Hamacher[47], G.Hamel De Monchenault[36], W.Hao[28], F.J.Harris[31], B.W.Heck[7], T.Henkes[7], J.J.Hernandez[44], P.Herquet[2], H.Herr[7], T.L.Hessing[20], I.Hietanen[12], C.O.Higgins[20], E.Higon[44], H.J.Hilke[7], S.D.Hodgson[31], T.Hofmokl[46], R.Holmes[1], S-O.Holmgren[40], D.Holthuizen[28], P.F.Honore[6], J.E.Hooper[27], M.Houlden[20], J.Hrubec[45], P.O.Hulth[40], K.Hultqvist[40], P.Ioannou[3], D.Isenhower[7], P-S.Iversen[4], J.N.Jackson[20], P.Jalocha[15], G.Jarlskog[22], P.Jarry[36], B.Jean-Marie[17], E.K.Johansson[40], D.Johnson[20], M.Jonker[7], L.Jonsson[22], P.Juillot[8], G.Kalkanis[3], G.Kalmus[34], F.Kapusta[21], M.Karlsson[7], E.Karvelas[9], S.Katsanevas[3], E.C.Katsoufis[29], R.Keranen[12], J.Kesteman[2], B.A.Khomenko[13], N.N.Khovanski[13], B.King[20], N.J.Kjaer[7], H.Klein[7], W.Klempt[7], A.Klovning[4], P.Kluit[28], J.H.Koehne[14], B.Koene[28], P.Kokkinias[9], M.Kopf[14], K.Korcyl[15], A.V.Korytov[13], V.Kostioukhine[39], C.Kourkoumelis[3], O.Kouznetsov[13], P.H.Kramer[47], J.Krolikowski[46], I.Kronkvist[22], J.Krstic[31], U.Kruener-Marquis[47], W.Krupinski[15], K.Kulka[43], K.Kurvinen[12], C.Lacasta[44], C.Lambropoulos[9], J.W.Lamsa[1], L.Lanceri[42], V.Lapin[39], J-P.Laugier[36], R.Lauhakangas[12], G.Leder[45], F.Ledroit[11], R.Leitner[7], Y.Lemoigne[36], J.Lemonne[2], G.Lenzen[47], V.Lepeltier[17], A.Letessier-Selvon[21], J.M.Levy[8], E.Lieb[47], D.Liko[45], E.Lillethun[4], J.Lindgren[12], R.Lindner[47], A.Lipniacka[46], I.Lippi[32], B.Loerstad[22], M.Lokajicek[13], J.G.Loken[31], A.Lopez-Fernandez[17], M.A.Lopez Aguera[38], M.Los[28], D.Loukas[9], J.J.Lozano[44], P.Lutz[6], L.Lyons[31], G.Maehlum[7], J.Maillard[6], A.Maltezos[9], F.Mandl[45], J.Marco[38], M.Margoni[32], J-C.Marin[7], A.Markou[9], T.Maron[47], S.Marti[44], L.Mathis[1], F.Matorras[38], C.Matteuzzi[26], G.Matthiae[35], M.Mazzucato[32], M.Mc Cubbin[20], R.Mc Kay[1], R.Mc Nulty[20], G.Meola[10], C.Meroni[26], W.T.Meyer[1], M.Michelotto[32], I.Mikulec[45], W.A.Mitaroff[45], G.V.Mitselmakher[13], U.Mjoernmark[22], T.Moa[40], R.Moeller[27], K.Moenig[7], M.R.Monge[10], P.Morettini[10], H.Mueller[14], W.J.Murray[34], B.Muryn[17], G.Myatt[31], F.Naraghi[21], F.L.Navarria[5], P.Negri[26], B.S.Nielsen[27], B.Nijjhar[20], V.Nikolaenko[39], P.Niss[40], V.Obraztsov[39], A.G.Olshevski[13], R.Orava[12], A.Ostankov[39], K.Osterberg[12], A.Ouraou[36], M.Paganoni[26], R.Pain[21], H.Palka[28], Th.D.Papadopoulou[29], L.Pape[7], A.Passeri[37], M.Pegoraro[32], J.Pennanen[12], V.Perevozchikov[39], M.Pernicka[45], A.Perrotta[5], A.Petrolini[10], F.Pierre[36], M.Pimenta[19], O.Pingot[2], M.E.Pol[7], G.Polok[15], P.Poropat[42], P.Privitera[14], A.Pullia[26], D.Radojicic[31], S.Ragazzi[26], P.N.Ratoff[18], A.L.Read[30], N.G.Redaelli[26], M.Regler[45], D.Reid[20], P.B.Renton[31], L.K.Resvanis[3], F.Richard[17], M.Richardson[20], J.Ridky[13], G.Rinaudo[41], I.Roditi[16], A.Romero[41], I.Roncagliolo[10], P.Ronchese[32], C.Ronnqvist[12], E.I.Rosenberg[1], S.Rossi[7], U.Rossi[5], E.Rosso[7], P.Roudeau[17], T.Rovelli[5], W.Ruckstuhl[28], V.Ruhlmann[36], A.Ruiz[38], K.Rybicki[15], H.Saarikko[12], Y.Sacquin[36], G.Sajot[11], J.Salt[44], J.Sanchez[24], M.Sannino[10], S.Schael[14], H.Schneider[14], M.A.E.Schyns[47], G.Sciolla[41], F.Scuri[42], A.M.Segar[31], R.Sekulin[34], M.Sessa[42], G.Sette[10], R.Seufert[14], R.C.Shellard[33], I.Siccama[28], P.Siegrist[36], S.Simonetti[10],

F.Simonetto[32], A.N.Sisakian[13], T.B.Skaali[30], G.Skjevling[30], G.Smadja[36,23], G.R.Smith[34], R.Sosnowski[46], T.S.Spassoff[11], E.Spiriti[37], S.Squarcia[10], H.Staeck[47], C.Stanescu[37], S.Stapnes[30], G.Stavropoulos[9], F.Stichelbaut[2], A.Stocchi[17], J.Strauss[45], J.Straver[7], R.Strub[8], M.Szczekowski[46], M.Szeptycka[46], P.Szymanski[46], T.Tabarelli[26], S.Tavernier[2], O.Tchikilev[39], G.E.Theodosiou[9], A.Tilquin[25], J.Timmermans[28], V.G.Timofeev[13], L.G.Tkatchev[13], T.Todorov[8], D.Z.Toet[28], O.Toker[12], E.Torassa[41], L.Tortora[37], M.T.Trainor[31], D.Treille[7], U.Trevisan[10], W.Trischuk[7], G.Tristram[6], C.Troncon[26], A.Tsirou[7], E.N.Tsyganov[13], M.Turala[15], M-L.Turluer[36], T.Tuuva[12], I.A.Tyapkin[13], M.Tyndel[34], S.Tzamarias[7], S.Ueberschaer[47], O.Ullaland[7], V.Uvarov[39], G.Valenti[5], E.Vallazza[41], J.A.Valls Ferrer[44], C.Vander Velde[2], G.W.Van Apeldoorn[28], P.Van Dam[28], W.K.Van Doninck[2], J.Varela[19], P.Vaz[7], G.Vegni[26], L.Ventura[32], W.Venus[34], F.Verbeure[2], L.S.Vertogradov[13], D.Vilanova[36], L.Vitale[12], E.Vlasov[39], S.Vlassopoulos[29], A.S.Vodopyanov[13], M.Vollmer[47], S.Volponi[5], G.Voulgaris[3], M.Voutilainen[12], V.Vrba[37], H.Wahlen[47], C.Walck[40], F.Waldner[42], M.Wayne[1], A.Wehr[47], M.Weierstall[47], P.Weilhammer[7], J.Werner[47], A.M.Wetherell[7], J.H.Wickens[2], J.Wikne[30], G.R.Wilkinson[31], W.S.C.Williams[31], M.Winter[8], D.Wormald[30], G.Wormser[17], K.Woschnagg[43], N.Yamdagni[40], P.Yepes[7], A.Zaitsev[39], A.Zalewska[15], P.Zalewski[17], D.Zavrtanik[7], E.Zevgolatakos[9], G.Zhang[47], N.I.Zimin[13], M.Zito[36], R.Zitoun[21], R.Zukanovich Funchal[6], G.Zumerle[32], J.Zuniga[44]

[1] Ames Laboratory and Department of Physics, Iowa State University, Ames IA 50011, USA
[2] Physics Department, Univ. Instelling Antwerpen, Universiteitsplein 1, B-2610 Wilrijk, Belgium
and IIHE, ULB-VUB, Pleinlaan 2, B-1050 Brussels, Belgium
and Service de Phys. des Part. Elém., Faculté des Sciences, Université de l'Etat Mons, Av. Maistriau 19, B-7000 Mons, Belgium
[3] Physics Laboratory, University of Athens, Solonos Str. 104, GR-10680 Athens, Greece
[4] Department of Physics, University of Bergen, Allégaten 55, N-5007 Bergen, Norway
[5] Dipartimento di Fisica, Università di Bologna and INFN, Via Irnerio 46, I-40126 Bologna, Italy
[6] Collège de France, Lab. de Physique Corpusculaire, 11 pl. M. Berthelot, F-75231 Paris Cedex 05, France
[7] CERN, CH-1211 Geneva 23, Switzerland
[8] Centre de Recherche Nucléaire, IN2P3 - CNRS/ULP - BP20, F-67037 Strasbourg Cedex, France
[9] Institute of Nuclear Physics, N.C.S.R. Demokritos, P.O. Box 60228, GR-15310 Athens, Greece
[10] Dipartimento di Fisica, Università di Genova and INFN, Via Dodecaneso 33, I-16146 Genova, Italy
[11] Institut des Sciences Nucléaires, Université de Grenoble 1, F-38026 Grenoble, France
[12] Research Institute for High Energy Physics, SEFT, Siltavuorenpenger 20 C, SF-00170 Helsinki, Finland
[13] Joint Institute for Nuclear Research, Dubna, Head Post Office, P.O. Box 79, 101 000 Moscow, USSR.
[14] Institut für Experimentelle Kernphysik, Universität Karlsruhe, Postfach 6980, D-7500 Karlsruhe 1, FRG
[15] High Energy Physics Laboratory, Institute of Nuclear Physics, Ul. Kawiory 26 a, PL-30055 Krakow 30, Poland
[16] Centro Brasileiro de Pesquisas, rua Xavier Sigaud 150, RJ-22290 Rio de Janeiro, Brazil
[17] Université de Paris-Sud, Lab. de l'Accélérateur Linéaire, Bat 200, F-91405 Orsay, France
[18] School of Physics and Materials, University of Lancaster - Lancaster LA1 4YB, UK
[19] LIP, Av. E. Garcia, 14 and Inst. Sup. Te'cnico, Univ. Te'cnica de Lisboa, Av. R. Pais, P-1000 Lisbon, Portugal
[20] Department of Physics, University of Liverpool, P.O. Box 147, GB - Liverpool L69 3BX, UK
[21] LPNHE, Universités Paris VI et VII, Tour 33 (RdC), 4 place Jussieu, F-75230 Paris Cedex 05, France
[22] Department of Physics, University of Lund, Sölvegatan 14, S-22363 Lund, Sweden
[23] Université Claude Bernard de Lyon, 43 Bd du 11 Novembre 1918, F-69622 Villeurbanne Cedex, France
[24] Universidad Complutense, Avda. Complutense s/n, E-28040 Madrid, Spain
[25] Univ. d'Aix - Marseille II - Case 907 - 70, route Léon Lachamp, F-13288 Marseille Cedex 09, France
[26] Dipartimento di Fisica, Università di Milano and INFN, Via Celoria 16, I-20133 Milan, Italy
[27] Niels Bohr Institute, Blegdamsvej 17, DK-2100 Copenhagen 0, Denmark
[28] NIKHEF-H, Postbus 41882, NL-1009 DB Amsterdam, The Netherlands
[29] National Technical University, Physics Department, Zografou Campus, GR-15773 Athens, Greece
[30] Physics Department, University of Oslo, Blindern, N-1000 Oslo 3, Norway
[31] Nuclear Physics Laboratory, University of Oxford, Keble Road, GB - Oxford OX1 3RH, UK
[32] Dipartimento di Fisica, Università di Padova and INFN, Via Marzolo 8, I-35131 Padua, Italy
[33] Depto. de Fisica, Pontificia Univ. Católica, C.P. 38071 RJ-22453 Rio de Janeiro, Brazil
[34] Rutherford Appleton Laboratory, Chilton, GB - Didcot OX11 OQX, UK
[35] Dipartimento di Fisica, Università di Roma II and INFN, Tor Vergata, I-00173 Rome, Italy
[36] CEN-Saclay, DPhPE, F-91191 Gif-sur-Yvette Cedex, France
[37] Istituto Superiore di Sanità, Ist. Naz. di Fisica Nucl. (INFN), Viale Regina Elena 299, I-00161 Rome, Italy
[38] Facultad de Ciencias, Universidad de Santander, av. de los Castros, E - 39005 Santander, Spain
[39] Inst. for High Energy Physics, Serpukow P.O. Box 35, Protvino, (Moscow Region), USSR.
[40] Institute of Physics, University of Stockholm, Vanadisvägen 9, S-113 46 Stockholm, Sweden
[41] Dipartimento di Fisica Sperimentale, Università di Torino and INFN, Via P. Giuria 1, I-10125 Turin, Italy
[42] Dipartimento di Fisica, Università di Trieste and INFN, Via A. Valerio 2, I-34127 Trieste, Italy
and Istituto di Fisica, Università di Udine, I-33100 Udine, Italy
[43] Department of Radiation Sciences, University of Uppsala, P.O. Box 535, S-751 21 Uppsala, Sweden
[44] Inst. de Fisica Corpuscular IFIC, Centro Mixto Univ. de Valencia-CSIC, and Departamento de Fisica Atomica Molecular y Nuclear, Univ. de Valencia, Avda. Dr. Moliner 50, E-46100 Burjassot (Valencia), Spain
[45] Institut für Hochenergiephysik, Österr. Akad. d. Wissensch., Nikolsdorfergasse 18, A-1050 Vienna, Austria
[46] Inst. Nuclear Studies and, University of Warsaw, Ul. Hoza 69, PL-00681 Warsaw, Poland
[47] Fachbereich Physik, University of Wuppertal, Postfach 100 127, D-5600 Wuppertal 1, FRG

1 Introduction

The Large Electron Positron collider, LEP, is well suited for tau lepton studies [1]. The decay $Z \to \tau^+\tau^-$ has a clean signature consisting of two back-to-back jets of typically one or three charged particles plus undetected neutrino(s), often accompanied by other neutral particles, thus making possible high-efficiency, low-background studies. At LEP one can study both the tau decay properties and its electroweak couplings to the Z boson.

Precise measurements of the branching ratios $\tau^- \to e^-\bar{\nu}_e\nu_\tau$ and $\tau^- \to \mu^-\bar{\nu}_\mu\nu_\tau$ can help to clarify the long-standing two standard deviations discrepancy [2,3] between the world-average measured $\tau^- \to e^-\bar{\nu}_e\nu_\tau$ branching ratio [3,4] and the value expected from the world average measured lifetime [3,5] and mass [6] through the relation

$$BR(\tau^- \to e^-\bar{\nu}_e\nu_\tau) = \left(\frac{\mathrm{G}_\tau}{\mathrm{G}_\mu}\right)^2 \left(\frac{\mathrm{m}_\tau}{\mathrm{m}_\mu}\right)^5 \left(\frac{\tau_\tau}{\tau_\mu}\right) \tag{1}$$

where $\tau_{\mu,\tau}$ and $\mathrm{m}_{\mu,\tau}$ are the lifetimes and masses of the muon and tau respectively and $\mathrm{G}_{\mu,\tau}$ are the Fermi constants determined from muon and tau decay [7]. In addition, a measurement of the leptonic branching ratios can be used to estimate the value of the strong coupling constant, $\alpha_s(m_\tau)$ [8]. This is obtained using the ratio

$$R^\tau_{had} = \frac{\Gamma(\tau^- \to hadrons\ \nu_\tau)}{\Gamma(\tau^- \to e^-\bar{\nu}_e\nu_\tau)} = \frac{1 - BR(\tau^- \to e^-\bar{\nu}_e\nu_\tau) - BR(\tau^- \to \mu^-\bar{\nu}_\mu\nu_\tau)}{BR(\tau^- \to e^-\bar{\nu}_e\nu_\tau)}. \tag{2}$$

The perturbative QCD contribution to R^τ_{had} can be expressed as a power series in α_s and is known to order α_s^3 [9].

The electroweak couplings of the tau to the Z boson can be determined by studying the tau decay products. The fermions produced in high energy e^+e^- annihilations through Z creation and decay are polarized due to the different strengths of the couplings of the neutral boson to left-handed and right-handed fermions. The difference in the cross section for producing left-handed fermions relative to the cross section for producing right-handed fermions is specified by a variable called helicity asymmetry. In the high energy limit where the mass of the fermion can be neglected, the helicity of the fermions produced in Z decays is a good quantum number. The helicity asymmetry of the anti-fermion has the same magnitude and opposite sign to that of the fermion.

Due to parity violation in tau decays, its decay products can be used as analyzers of its polarization. Ignoring the small contribution from one photon exchange and neglecting the effect of variations in centre-of-mass energy around the Z resonance, one obtains for the tau polarization P_τ, averaged over all tau production angles,

$$P_\tau \simeq \frac{-2v_\tau a_\tau}{v_\tau^2 + a_\tau^2}, \tag{3}$$

where v_τ and a_τ are the vector and axial coupling constants of the tau lepton to the Z. In the Standard Model, the coupling constants can be expressed as $v_\tau = 4\sin^2\theta_W(m_Z^2) - 1$ and $a_\tau = -1$. A detailed discussion can be found in [10].

This paper presents a study of the tau lepton decay channels $\tau^- \to e^-\bar{\nu}_e\nu_\tau$, $\tau^- \to \mu^-\bar{\nu}_\mu\nu_\tau$, $\tau^- \to \pi^-(K^-)\nu_\tau$ (π and K particles are not separated), $\tau^- \to \rho^-\nu_\tau$ and their charge conjugates using the DELPHI detector at LEP. From the measurement of the leptonic branching ratios combined with the world averaged value of the tau lifetime the ratio of the tau to the muon Fermi couplings constants $\mathrm{G}_\tau/\mathrm{G}_\mu$ is obtained. From the measurement of the electronic and muonic branching ratios the value of the strong

coupling constant can be determined. Finally, from a measurement of the tau polarization a value of the electroweak mixing parameter is derived.

For this analysis, simulated $e^+e^- \to \tau^+\tau^-$ events were generated using the Monte Carlo generator KORALZ [11] which includes QED radiative effects in the production and decay processes of the tau leptons. For background studies samples of $e^+e^- \to \mu^+\mu^-$ events were produced using KORALZ, $e^+e^- \to e^+e^-$ events using BABAMC [12], $e^+e^- \to$ *hadrons* events with LUND 7.2 [13] and $e^+e^- \to (e^+e^-)X$ events with the Berends-Daverveldt-Kleiss generator [14].

The organization of the paper is as follows: section 2 is devoted to a brief description of the detector. The event preselection is discussed in section 3. Section 4 gives details of the calculation of the branching ratios. Section 5 explains the technique used to measure the tau polarization. Sections 6 to 9 describe the measurement of the tau decay to the four exclusive states considered. Finally in section 10 the results are summarised and discussed.

2 Detector

A detailed description of the DELPHI apparatus can be found in [15]. In the DELPHI coordinate system, θ is the polar angle defined with respect to the z axis which is taken as the electron beam direction and ϕ is the azimuthal angle about this axis. For the present analysis the following parts of the detector were relevant:

1. for the measurement of charged particles the MicroVertex Detector (MVD), the Inner Detector (ID), the Time Projection Chamber (TPC), and the Outer Detector (OD);
2. for the measurement of the electromagnetic energy the High-density Projection Chamber (HPC); this detector was also used for identifying minimum ionizing particles;
3. for the measurement of the hadronic energy and muon identification the Hadron Calorimeter (HCAL).
4. for muon identification the barrel muon chambers (MUB). Most of the solid angle in the barrel is covered by 2 layers of MUB with the rest having either 1 or 3 layers of coverage, each layer consisting of two overlapping sets of chambers.
5. for the trigger, besides the detectors mentioned above, the barrel Time-Of-Flight counters (TOF), the endcap scintillators (HOF) and a scintillator layer embedded in the HPC;
6. for the measurement of the luminosity the Small Angle Tagger (SAT).

The ID and TPC cover the angular range $20^0 < \theta < 160^0$, the OD covers the range $43^0 < \theta < 137^0$. Penetrating muons with a polar angle in the range $51^0 < \theta < 129^0$ can traverse 4 layers of HCAL and up to 3 layers of MUB. In the rest of the barrel region there are 3 layers of HCAL. The HPC has the same angular coverage as the OD.

Within the barrel region the momentum resolution obtained for muons with momentum of 46 GeV/c was $\sigma_{\rm p}/{\rm p} = 0.08$. The energy resolutions $(\sigma_{\rm E}/{\rm E})$ of the HPC for 46 GeV electrons is 0.08. The HCAL energy resolution is $1.0/\sqrt{{\rm E(GeV)}}$.

3 Event Preselection

Before identifying exclusive τ decays an enriched sample of $\tau^+\tau^-$ events was selected with a loose "filter". The selection was optimized to minimize distortions of the momentum spectrum and decay mode dependent biases. It proceeded in two steps. In the first step, Z candidates decaying into lepton pairs were selected. This selection has been described in detail elsewhere [16]. It demanded a configuration of two back to back jets with one particle in one jet and up to five particle in the other. The isolation angle, defined as the angle between the isolated particle and the closest particle in the recoiling jet was required to be greater than 150^0. A charged particle had to satisfy the following conditions:

1. momentum larger than 200 MeV/c;
2. distance of closest approach of the track to the beam axis less than 1.5 cm;
3. distance of closest approach to the nominal interaction point along the beam direction less than 4.5 cm.

These conditions rejected hadronic events. The low energy background arising from beam-gas, beam-wall and two-photon interactions was suppressed by demanding that at least one charged particle in the event had a momentum greater than 3 GeV/c. In order to ensure good understanding of the detector response, the acceptance for the leptonic events was restricted to the barrel region covering the angular acceptance $43^0 < \theta < 137^0$.

In the second step tau pairs were partially separated from the other two leptonic channels. This was achieved by taking advantage of the presence of undetected neutrinos in all tau decay modes, as opposed to $e^+e^- \rightarrow e^+e^-$ and $e^+e^- \rightarrow \mu^+\mu^-$ events which are characterized by their low acollinearity and high visible momentum and energy. The following selection criteria were applied:

1. The event acollinearity had to be greater than 0.5^0.
2. The variable $E_R = \sqrt{E_1^2 + E_2^2}/E_{beam}$, where E_1 is the electromagnetic energy associated with the isolated charged particle and E_2 is the total electromagnetic energy associated with the charged particle(s) in the hemisphere opposite to the isolated particle and E_{beam} is the beam energy had to satisfy the condition $E_R < 1.2$.
3. The variable $P_R = \sqrt{P_1^2 + P_2^2}/E_{beam}$, where P_1 is the momentum of the isolated charged particle and P_2 is the resultant momentum of the recoiling jet had to satisfy the requirement $P_R < 1.3$.

These cuts suppress the $e^+e^- \rightarrow e^+e^-$ and $e^+e^- \rightarrow \mu^+\mu^-$ backgrounds while affecting only slightly the $\tau^+\tau^-$ sample. Fig 1(a) shows E_R for simulated tau pairs and $e^+e^- \rightarrow e^+e^-$ events. Fig 1(b) shows P_R for simulated tau pairs and $e^+e^- \rightarrow \mu^+\mu^-$ events. Fig 1(c) shows the average efficiency of the filter as a function of the momentum of the particle of maximum momentum in the event, P_{max}. Small decay mode dependent biases lead to slightly different acceptances for the individual channels considered: $\tau^- \rightarrow e^-\bar{\nu}_e\nu_\tau$ $82.8 \pm 0.8\%$; $\tau^- \rightarrow \mu^-\bar{\nu}_\mu\nu_\tau$ $87.2 \pm 0.8\%$; $\tau^- \rightarrow \pi^-(K^-)\nu_\tau$ $84.1 \pm 0.8\%$; $\tau^- \rightarrow \rho^-\nu_\tau$ $83.8 \pm 0.8\%$.

4 Calculation of Branching Ratios

Starting from the tau-enriched sample a decay-mode-dependent selection is performed. The branching ratio for a specific channel is then calculated from the expression

$$BR(\tau \to i) \;=\; \frac{N_i^{obs}}{2 \cdot N_{\tau^+\tau^-}} \cdot \frac{1 - f_i^{bkg}}{\epsilon_i} \tag{4}$$

where N_i^{obs} is the number of decays passing the selection criteria for the decay mode i, f_i^{bkg} is the estimated background fraction in the sample, and ϵ_i is the overall efficiency to select $\tau \to i$ decays normalized to the full solid angle. $N_{\tau^+\tau^-}$ is the number of tau pairs in the full solid angle computed from a previous measurement of the tau pair cross section [16] using the relation

$$N_{\tau^+\tau^-} \;=\; \sum_j \frac{N_{line}^j}{\epsilon_{line}^j} \, (1 - b_{line}^j) \, f_{rs} \tag{5}$$

where the index $j = 1,7$ runs over the seven energy points measured in the line scan, N_{line}^j is the number of decays found per energy point in the line scan, ϵ_{line}^j is the efficiency of the tau pair selection used for the linescan, b_{line}^j is the background for the linescan selection, and f_{rs} takes into account the slightly different run selection for this analysis and the line scan analysis. We obtain $N_{\tau^+\tau^-} = 4884$. A common fractional systematic error of 2.4% is included in all branching fraction measurements arising from the statistical uncertainty in N_{line}^j (2.1%) and the uncertainties in ϵ_{line} (1.0%), b_{line} (0.6%) and f_{rs} (0.4%).

The systematic errors in the computation of the branching ratios are mainly due to the uncertainties in the background estimate and in the selection efficiency for the different channels studied. In the case of the leptonic decays of the tau, both the efficiency and the background can be measured from the data themselves or the data can be used to correct the Monte Carlo simulation. This is more difficult to do for the hadronic channels, in particular for the decay $\tau^- \to \rho^- \nu_\tau$, where one has to rely heavily on the simulation. In this case the errors were estimated by varying the selection variable cuts within resonable values.

5 Tau Polarization

The angular distribution of the tau decay products in the tau rest frame is correlated with the tau spin and affects the momentum spectrum of the decay products in the laboratory frame. This momentum distribution can therefore be used to measure the tau polarization. Neglecting radiative corrections and the masses of the decay products, the standard model prediction for the momentum spectrum in the decay $\tau^- \to l^- \bar{\nu}_l \nu_\tau$ (where $l = e, \mu$) is

$$\frac{1}{N_l}\frac{dN_l}{dx_l} \;=\; \frac{1}{3}[5 - 9x_l^2 + 4x_l^3 + P_\tau(1 - 9x_l^2 + 8x_l^3)], \tag{6}$$

while for the decay $\tau^- \to \pi^-(K^-)\nu_\tau$,

$$\frac{1}{N_\pi}\frac{dN_\pi}{dx_\pi} \;=\; 1 + P_\tau(2x_\pi - 1), \tag{7}$$

where x_l, x_π are the momenta of the emitted lepton or pion (kaon) divided by the beam momentum.

In order to measure the tau polarization, a linear combination of simulated event distributions for positive and negative helicity have been fitted to the corrected momentum spectra of the muon produced in the decay $\tau^- \to \mu^- \bar{\nu}_\mu \nu_\tau$ and the pion produced in the decay $\tau^- \to \pi^- \nu_\tau$ while for the decay $\tau^- \to e^- \bar{\nu}_e \nu_\tau$ the corrected spectrum of energy deposited in the calorimeter has been fitted to reduce effects due to radiation of photons.

The corrected binned momentum or energy distribution to be fitted is obtained from the observed distribution via the transformation

$$N_i^{corr} = \frac{1}{\epsilon_i} \cdot \sum_j U_{ij} \cdot N_j^{obs} \cdot (1 - f_j^{bkg}) \tag{8}$$

where the corrections due to the centre-of-mass energy dependence of the value of P_τ have been neglected since they are negligible at this level of statistical precision. U_{ij} is the unfolding matrix that relates the number of events in the bin j of the observed distribution to the number of events in the bin i of the corrected distribution, ϵ_i is the efficiency in bins of the corrected distribution and f_j^{bkg} is the estimated background in bins of the observed distribution. U_{ij} is calculated from Monte Carlo simulation. The small uncertainty on the estimation of U_{ij} arising from the fact that the calculation is not completely independent of the value of P_τ assumed in the Monte Carlo simulation is negligible compared with the major sources of systematic errors, which are discussed in the corresponding sections.

In the decay $\tau^- \to \rho^- \nu_\tau$ the vector structure of the ρ meson allows two different helicity states, 0 or -1, depending on the component of the spin of the tau along the decay axis. This implies a reduction in the sensitivity of the momentum spectrum of the ρ to P_τ, compared with that appearing in Eq. 3, by the factor [7,17]

$$\alpha = \frac{m_\tau^2 - 2m_\rho^2}{m_\tau^2 + 2m_\rho^2} \tag{9}$$

Thus, since $\alpha \sim 0.46$, the sensitivity of this channel to P_τ would be poorer than for the channel $\tau^- \to \pi^- \nu_\tau$ if the momentum spectrum were fitted. However, the sensitivity to P_τ can be regained [18,19] by measuring the helicity of the spin-1 system. To this end the final state can be defined by two angles: the angle θ_τ of the ρ momentum in the τ rest frame

$$\cos\theta_\tau = \frac{2x_\rho - 1 - m_\rho^2/m_\tau^2}{1 - m_\rho^2/m_\tau^2}, \tag{10}$$

and the angle θ_ρ which characterizes the decay distribution of the ρ into final state pions

$$\cos\theta_\rho = \frac{m_\rho}{\sqrt{m_\rho^2 - 4m_\pi^2}} \frac{E_\pi - E_{\pi^0}}{|\vec{P}_\pi + \vec{P}_{\pi^0}|}. \tag{11}$$

To measure the tau polarization, a linear combination of simulated event distributions for positive and negative helicities was fitted to the corrected distributions for the angles θ_τ and θ_ρ with P_τ taken as a free parameter.

6 The $\tau^- \to e^- \bar{\nu}_e \nu_\tau$ channel

Candidates for the decay $\tau^- \to e^- \bar{\nu}_e \nu_\tau$ are characterized by an isolated charged particle identified as an electron. In DELPHI, electrons are identified using calorimetric information from the HPC and the energy deposited per unit length (dE/dx) in the TPC.

To identify an electron in the HPC use was made of its good spatial resolution and high granularity. The mean longitudinal profile of the energy deposition in an electromagnetic cascade can be described [20] by a gamma distribution

$$dE/dt \;=\; E_0 \cdot b \cdot \frac{(bt)^{a-1}e^{-bt}}{\Gamma(a)} \qquad (12)$$

where t is the shower depth expressed in radiation lengths, E_0 is the shower energy and a and b are empirical parameters. In this parametrization, the maximum of the shower $t_{max} = a/b$ and the scale factor $L = 1/b$ are both logarithmically dependent on E_0. To identify a particle showering in the HPC as an electron, the theoretical expression above is used to predict the expected energy deposited per layer, and the χ^2 of the difference between the predicted and the actual value of the energy deposited per layer is computed. The momentum of the track is used as an approximation for E_0. The χ^2 computed in this way is used as identification variable EX. Details of the algorithm can be found in [21].

The electron identification efficiency was measured with a test sample of events in which a primary electron radiates a virtual photon that Compton-scatters against the other electron. These events were selected by requiring only one charged particle in the barrel region of the detector and more than 15 GeV energy deposited in the FEMC or the SAT. In addition $e^+e^- \to e^+e^-$ events were used to cover the full momentum range. The signature of the hadronic background was also studied with a test sample of hadrons from τ decays obtained by requiring single tracks with a dE/dx deposition in the TPC incompatible ($< 0.5\%$ probability) with that expected for an electron and with more than 1 GeV energy deposited in the HPC. With this sample one can measure the fraction of hadrons that are identified as an electron for a given value of EX. Monte Carlo simulation has been used to correct for the fact that the hadron sample has a different momentum distribution than the potential background from hadronic tau decays. The variable REL is defined as the normalized difference between the dE/dx measured and that expected for an electron. A cut on $REL < -2$ provides a hadronic sample virtually free from electron contamination. This is illustrated in Fig 2(a), where the REL distribution is shown for single tracks of more than 2 GeV/c momentum together with the Monte Carlo prediction for electrons. The variable EX is shown in Fig. 2(b) for the electron and hadron data samples. Demanding $EX < 3$ one obtains an electron identification efficiency of $96 \pm 1\%$ in good agreement with the Monte Carlo prediction. The procedure to select $\tau^- \to e^- \bar{\nu}_e \nu_\tau$ candidates was then as follows.

1. The event had to contain a single charged track in one hemisphere with a momentum greater than 2 GeV/c and an energy deposition greater than 1 GeV in the HPC.
2. The track had to be identified as an electron in the HPC ($EX < 3$) with a value of dE/dx in the TPC compatible with that expected from an electron ($|REL| < 2$).
3. The total energy of the neutral particles not associated to the charged track in a cone of 30^0 around its direction was required to be less than 5 GeV.
4. The energy deposited in the hadronic calorimeter had to be less than 1 GeV.

The efficiency of these selection criteria was found to be $72.3 \pm 1.0\%$. The electron test sample was used to correct the Monte Carlo calculation bin by bin. The integrated correction was 0.914 ± 0.013. The major discrepancies between data and the Monte Carlo simulation were found in the track-shower linking efficiency of the HPC and in the fraction of electrons depositing more than 1 GeV in the hadronic calorimeter. The background arising from other tau decays was estimated independently from Monte Carlo simulation

and from the hadron data sample to be $4.5 \pm 1.0\%$. The main contributions to this background were the decay modes $\tau^- \to \rho^- \nu_\tau$ and $\tau^- \to \pi^- \nu_\tau$.

Once an electron was identified in the event, additional conditions were imposed to suppress the background arising from $e^+e^- \to e^+e^-$ events and two-photon events. The background due to $e^+e^- \to e^+e^-$ was suppressed using the fact that these events should deposit a large amount of electromagnetic energy in the HPC. However, $e^+e^- \to e^+e^-$ events in which one of the electrons is near a gap between modules of the HPC can deposit considerably less energy. Therefore events where either of the particles entered the HPC within 1^0 of a gap were rejected. To further reduce the $e^+e^- \to e^+e^-$ background the total electromagnetic energy in the event was required to be less than $1.2E_{beam}$ except when the particle with the highest momentum in the opposite hemisphere entered the HPC within 2^0 of a gap in which case this cut was tightened to $1.1E_{beam}$ and the event acoplanarity was required to be greater than 1^0. These selection requirements reduced the $e^+e^- \to e^+e^-$ background to $0.7 \pm 0.3\%$.

The background due to two-photon interactions was further suppressed by requiring the missing transverse momentum in the event to be greater than 0.5 GeV/c and the event acollinearity to be less than 15^0. These criteria reduced the two-photon background to $0.8 \pm 0.4\%$.

These selection criteria resulted in a sample of 554 $\tau^- \to e^- \bar{\nu}_e \nu_\tau$ candidates. The overall efficiency of identification of $\tau^- \to e^- \bar{\nu}_e \nu_\tau$ decays inside the fiducial volume was found to be $44.4 \pm 1.0\%$. To measure the polarization, the distribution of electromagnetic energy deposited in a 30^0 cone about the track E_e was used in preference to the particle momentum as this had smaller corrections from radiated photons. The efficiency is shown plotted in bins of normalized energy $X_e = E_e/E_{beam}$, in Fig. 3(a). In Fig. 3(b) the resulting electron candidate energy spectrum is shown superimposed with the Monte Carlo prediction (for $P_\tau = -0.16$) for both the signal and the background. In Fig. 3(c) the corrected spectrum is shown together with the fit. A value for the tau polarization of

$$P_\tau = -0.12 \pm 0.22 \pm 0.08$$

was obtained. The major sources of systematic errors were: the dependence of the identification efficiency with the energy(0.05); the background subtraction (0.03); the uncertainty in the energy resolution (0.04); the Monte Carlo statistics (0.03). A value of the branching ratio

$$BR(\tau^- \to e^- \bar{\nu}_e \nu_\tau) = 18.6 \pm 0.8(stat) \pm 0.6(sys)\%$$

was obtained. Sources of systematic error included the selection efficiency (0.4%) and background subtraction (0.2%).

7 The $\tau^- \to \mu^- \bar{\nu}_\mu \nu_\tau$ channel

Candidates for the decay $\tau^- \to \mu^- \bar{\nu}_\mu \nu_\tau$ are characterized by an isolated charged particle identified as a muon. A muon is a Minimum Ionizing Particle (MIP) in the HPC and HCAL and produces hits in the muon chambers. This can be used to achieve a high-efficiency, low-background muon identification. In addition, the efficiency of selection criteria based on one detector can be measured by selecting a muon sample using the other detectors or by using $\mu^+\mu^-$ events.

The cosmic-ray background was reduced by removing events with a 1-1 topology that satisfied either of the following conditions:

1. $|z_1 - z_2| > 3.0$ cm, where z_1 and z_2 are the z coordinates of the two tracks in the event at their points of closest approach to the beam axis. Due to the drift in z being in opposite directions for $+z$ and $-z$ in the TPC this is equivalent to requiring that the event be within a time interval of $\pm$ 110 ns relative to the bunch crossing time.
2. A time of arrival more than 25 ns from the time expected for a Z event, using the OD pattern recognition.

A study of these cuts using events in an extended vertex region showed the remnant cosmic background to be negligible, with no measureable loss of $\tau^+\tau^-$ events.

A charged particle was identified as a muon if it satisfied an AND of the following criteria:

1. The particle had to deposit less than 3 GeV energy in the HPC.
2. The total electromagnetic energy deposited in a cone of 30^0 around the track had to be less than 0.3 GeV.
3. The particle had to give a signal in the HCAL consistent with that expected from a muon. The total energy, E_{HCAL}, deposited by the particle in the HCAL had to satisfy the following cuts as a function of the track polar angle θ

   (a) For $55^0 < \theta < 88^0$, $E_{HCAL} < 10.0\ GeV/sin^2(\theta)$,
   (b) for $51^0 < \theta < 55^0$, $E_{HCAL} < 15.0\ GeV$,
   (c) and for $43^0 < \theta < 51^0$, $E_{HCAL} < 12.5\ GeV$.

   The variation is due to the change in depth of the material in HCAL as a function of polar angle. Fig. 4 shows the energy deposition in the HCAL for muons in dimuon events selected using a tight acollinearity cut and requiring that the particle in the opposite hemisphere has muon chamber hits.
4. (a) One or more hits in the muon chambers or
   (b) Any energy deposition in the outer layer(s) of HCAL. This was the fourth layer for $51^0 < \theta < 129^0$ and was defined as the sum of the third and fourth layers for $43^0 < \theta < 51^0$ and $129^0 < \theta < 137^0$.

The efficiency of these selection cuts was $89.9 \pm 2.0\%$ with good agreement between the Monte Carlo estimate and data using muons in $\mu^+\mu^-$ events. The background from other tau decays was calculated from Monte Carlo simulation and checked with a background free sample of pions obtained by requiring the positive identification of a $\tau^- \to \rho^-\nu_\tau$ decay. Simulation and data agree well, giving a background estimation of $2.3 \pm 1.0\%$, mainly from the $\tau^- \to \pi^-\nu_\tau$ channel.

Other major sources of background were $e^+e^- \to \mu^+\mu^-$ events and two-photon events. The two-photon background was suppressed by requiring the missing transverse momentum in the event to be greater than 0.5 GeV/c and the event acollinearity to be less than 15^0. These selection criteria reduce the two-photon background to $0.9 \pm 0.5\%$. An event was rejected as a $e^+e^- \to \mu^+\mu^-$ event if it satisfied any of the following conditions:

1. $P_R = \sqrt{P_1^2 + P_2^2}/E_{beam}$ greater than 1.2;
2. if the particle in the opposite hemisphere to the identified particle was consistent with being a muon as defined by the identification criterion (4) described above, and if either of the following two conditions were satisfied:

   (a) $P_{opp} > 0.7E_{beam}$
   (b) $min(P_{opp} + E_{cone}, P_\mu) > 0.6E_{beam}$;

P_{opp} is the momentum of the particle in the opposite hemisphere; E_{cone} is the energy deposited in a 30^0 cone about this particle and P_μ is the momentum of the identified muon: cut (b) removed the tail of radiative $e^+e^- \to \mu^+\mu^-$ events;

3. if the opposite hemisphere contains more than one charged particle and the particle with the highest momentum satisfies criterion (4) as discussed above: this removes background from $\mu^+\mu^-\gamma$ events where the photon has converted.

The efficiency for identifying a muon with selection criterion (4) was $97.1 \pm 0.6\%$. The fraction of muon and hadronic tau decays satisfying this condition was 21%. Both numbers showed good agreement between Monte Carlo and data. The positive identification of candidates makes it possible to suppress the $e^+e^- \to \mu^+\mu^-$ events while minimally distorting the $\tau^- \to \mu^-\bar{\nu_\mu}\nu_\tau$ spectrum and with negligible effect on the branching ratio measurement. The remaining background from $\mu^+\mu^-$ events was estimated to be $1.1 \pm 0.5\%$.

With these selection criteria the data sample contained 687 events. The overall efficiency of identification of $\tau^- \to \mu^-\bar{\nu_\mu}\nu_\tau$ decays inside the fiducial volume was found to be $59.9 \pm 1.1\%$. The efficiency is shown plotted in bins of normalized momentum $X_\mu = P_\mu/E_{beam}$ in Fig. 5(a). In Fig. 5(b) the muon candidate momentum spectrum is shown superimposed with the Monte Carlo prediction (for $P_\tau = -0.16$) for both the signal and the background. In Fig. 5(c) the corrected spectrum is shown together with the fit. A value for the tau polarization of

$$P_\tau = -0.05 \pm 0.18(stat) \pm 0.07(sys)$$

was obtained. The dominant systematic errors were: the dependence of the identification efficiency with the energy (0.02); background subtraction (0.05); the momentum resolution (0.03); the Monte Carlo statistics (0.03).

The branching ratio was calculated to be

$$BR(\tau^- \to \mu^-\bar{\nu_\mu}\nu_\tau) = 17.4 \pm 0.7(stat) \pm 0.6(sys)\%.$$

The systematic errors arose from the selection efficiency (0.5%) and background subtraction (0.2%).

8 The $\tau^- \to \pi^-(K^-)\nu_\tau$ channel

The identification of $\tau^- \to \pi^-(K^-)\nu_\tau$ decays is more difficult, since most other tau decay channels are potential sources of background. The separation of electrons and ρ's from pions relies on the fine granularity of the HPC. The separation of pions from muons requires the hadron calorimeter and the muon chambers. In this analysis the two major difficulties are, firstly, to remove background from $\tau^- \to \mu^-\bar{\nu_\mu}\nu_\tau$ while keeping good efficiency for high momentum pions which have a tendency to leave energy deposits deep in the HCAL or in the muon chambers, and secondly, to remove background from $\tau^- \to \rho^-\nu_\tau$ decays where the π^o is lost, either because it escapes through a gap between modules of the HPC or because it has too low an energy to be reconstructed. In order to achieve optimal separation between pions and muons the analysis was restricted to the region $52^0 < \theta < 128^0$ where the HCAL and the MUB have maximum redundancy.

A $\tau^- \to \pi^-(K^-)\nu_\tau$ candidate had to satisfy the following requirements:

1. The hemisphere had to contain a single charged particle with momentum greater than $0.1E_{beam}$.

2. The particle had to deposit energy in the HPC or the HCAL.
3. There should be no reconstructed neutral particles in a 30^0 cone around the particle. This rejects tau decays containing π^0's.
4. In order to reject electrons it was required that the particle deposits less than 350 MeV energy in the first 4 layers of the HPC. This corresponds to about 4 times the average energy deposition of a minimum ionizing particle.
5. The separation of pions from muons was achieved by rejecting all the particles that were identified as muons when at least one of the following conditions was fulfilled:
   (a) there were one or more hits associated to the track in the outer layer of the muon chambers.
   (b) if a particle with a polar angle θ left an energy deposition E_{HCAL} in the HCAL consistent with a minimum ionizing particle as defined by the cut

$$E_{HCAL} \; < \; N_{layers} \cdot 3.0 \; GeV \; / \; sin^2(\theta),$$

   and if it was identified as a muon using the the outer layer(s) of HCAL or the muon chambers as described under selection criterion (4) in section (7). N_{layers} is the number of layers in HCAL with an energy deposition greater than zero.

The overall efficiency to select $\tau^- \rightarrow \pi^-(K^-)\nu_\tau$ decays from the sample was computed by Monte Carlo simulation to be $34.7 \pm 2\%$, where the major contribution to the uncertainty arose from the poor knowledge of pion interactions in the HPC. The background from other tau decays was computed by Monte Carlo simulation to be $7 \pm 3\%$, due to: $\tau^- \rightarrow \mu^- \bar{\nu_\mu} \nu_\tau$ (3%); $\tau \rightarrow \pi \nu_\tau + n\pi^0$ (2%); $\tau \rightarrow K^* \nu_\tau$ (2%). The background from dimuon events was estimated to be $0.9 \pm 0.7\%$.

After the selection, 283 $\tau^- \rightarrow \pi^-(K^-)\nu_\tau$ candidates remained. The efficiency is shown plotted in bins of normalized momentum $X_\pi = P_\pi / E_{beam}$ in Fig. 6(a). In Fig. 6(b) the resulting pion candidate normalized momentum spectrum is shown superimposed with the Monte Carlo prediction (for $P_\tau = -0.16$) for both the signal and the background. In Fig. 6(c) the corrected spectrum is shown together with the fit. A value for the tau polarization of

$$P_\tau \; = \; -0.35 \pm 0.11 \pm 0.07$$

was obtained.

The dominant systematic errors were: the dependence of the identification efficiency with the energy (0.01); the background subtraction (0.06); the momentum resolution (0.03); the Monte Carlo statistics (0.03).

The measured branching ratio was found to be

$$BR(\tau^- \rightarrow \pi^-(K^-)\nu_\tau) = 11.9 \pm 0.7(stat) \pm 0.7(sys).\%$$

The systematic errors arose from uncertainties in the selection efficiency (0.6%) and background subtraction (0.3%).

9 The $\tau^- \rightarrow \rho^- \nu_\tau$ channel

The criteria used to select the decay $\tau^- \rightarrow \rho^- \nu_\tau$ were based on the good spatial resolution of the HPC. Since the π^0 produced in the decay $\rho \rightarrow \pi\pi^0$ decays into two photons, the ability to detect and separate electromagnetic showers is essential for this analysis. The ideal signature of the channel occurs when the two photons can be separated, their invariant mass reconstructed and found to be compatible with the mass of the π^0, and

the invariant mass of the $\pi^0 - \pi$ system found to be compatible with the ρ mass. This requires that both photons be identified in the HPC, which in turn requires the π^0 to have sufficiently low energy (typically around 5 GeV) so that the two photons separate enough to be reconstructed as two separate showers. Only about 40% of the candidate decays satisfied this requirement. In the case where an energetic π^0 decays into two photons which are too close to be separated as two independent neutrals in the HPC, the structure of the energy clusters in the first three layers of the HPC (about 4 radiation lengths) can be used to separate these two photons. When two such photon showers were identified inside a neutral cluster the invariant mass was computed by assigning half of the neutral energy to each of them. About 20% of all $\tau^- \to \rho^-\nu_\tau$ candidates had this topology, which was free of background. In about 60% of cases, therefore, one could impose the reconstruction of the π^0 mass in addition to the reconstruction of the ρ mass.

In the remaining 40% of the candidate $\tau^- \to \rho^-\nu_\tau$ decays, one of the photons was lost because it entered a gap in the HPC, or because it could not be reconstructed due to either a late conversion (i.e. in the outer wall of the TPC) into a electron-positron pair or to having an energy too low to be detected in the HPC. This topology appeared as one charged particle plus one photon. In order to reduce backgrounds, a cut was made on the invariant mass of the $\gamma - \pi$ system as discussed below.

The procedure used to select the candidate tau decays was as follows.

1. It was required that an isolated charged particle had one or two neutral showers of greater than 0.5 GeV energy in the surrounding 30^0 cone, that these showers started before the fourth layer of the HPC and that they deposited energy in at least three layers of the HPC.
2. The total electromagnetic energy in the event had to be less than $1.3E_{beam}$ and the momentum in the hemisphere opposite to the candidate had to be lower than $0.85E_{beam}$ to reject the $e^+e^- \to e^+e^-$ and $e^+e^- \to \mu^+\mu^-$ backgrounds.
3. To suppress the background coming from $\tau^- \to e^-\bar{\nu}_e\nu_\tau$, the track of the $\tau^- \to \rho^-\nu_\tau$ candidate was required to have the EX variable as defined in Section 6 greater than 1.5. Low momentum electrons which radiate a photon were eliminated by asking that, if the charged particle momentum was less than 5 GeV/c, the sum of the π^0 and the charged particle deposited energies divided by the charged particle momentum be outside the range between 0.5 and 1.5.

The events were then classified into two categories: 1) π + reconstructed π^0, 2) $\pi + \gamma$. In both cases, a minimum energy of 1.5 GeV was required for the neutral particle (γ or π^0). Fig. 7 shows the energy distribution of the neutral particle as defined above.

To select an event in category 1) the invariant mass of the two neutrals was required to be in the range $0.04\ \mathrm{GeV}/c^2 < m_{\pi^0} < 0.40\ \mathrm{GeV}/c^2$.

In both cases, the invariant mass of the $\pi - (\gamma\ or\ \pi^0)$ system was required to be in the range $0.5\ \mathrm{GeV}/c^2 < m_{\pi-(\gamma\ or\ \pi^0)} < 1.1\ \mathrm{GeV}/c^2$.

Fig. 8 and Fig. 9 show the reconstructed π^0 mass and the reconstructed ρ mass distributions respectively, superimposed with the Monte Carlo prediction. After these selections, 694 $\tau^- \to \rho^-\nu_\tau$ candidates remained. The overall efficiency inside the geometrical acceptance was computed by Monte Carlo simulation to be $41.2 \pm 2.0\%$. The background as determined by Monte Carlo simulation was $16 \pm 2\%$, mostly due to the $\tau \to \pi\pi^0\pi^0\nu$ and $\tau \to K^*\nu$ decay modes. Fig. 10 shows the distribution of the angles defined in Sect. 4 for Monte Carlo and data. A maximum likelihood fit gave

$$P_\tau = -0.24 \pm 0.09 \pm 0.07.$$

The main contributions to the systematic error arose from the uncertainties in the acceptance and the photon reconstruction efficiency (0.06), the background subtraction (0.02) and the Monte Carlo statistics (0.03).

The measured branching ratio was

$$BR(\tau^- \to \rho^- \nu_\tau) = 22.4 \pm 0.8(stat) \pm 1.3(sys)\%.$$

Systematic errors arose from: selection efficiency (1.1%); background subtraction (0.4%).

10 Conclusions

Table 1 summarizes the results obtained from the analysis of the different decay channels. The weighted mean of the measurements in the different decay channels gives an estimate for the tau polarization of

$$P_\tau \;=\; -0.24 \pm 0.07.$$

The statistical and systematic errors have been added in quadrature, neglecting small correlations between the systematic errors of the different decay modes. Using equation 3, a value of the ratio of the vector to the axial coupling constant of the tau to the Z of

$$\frac{v_\tau}{a_\tau} = 0.12 \pm 0.04$$

is obtained, thus yielding a value of the effective mixing angle

$$\sin^2\theta_W(m_Z^2) = 0.220 \pm 0.009\ ,$$

in agreement with the value for $\sin^2\theta_W(m_Z^2)$ of 0.2338 ± 0.0027 derived from the Z line shape and asymmetry measurement [16]. The present results are in good agreement with those published recently by the ALEPH [23] and OPAL [24] collaborations.

The observed electronic branching ratio of $18.6 \pm 0.8(stat) \pm 0.6(sys)\%$ agrees well with the value of $18.9 \pm 0.5\%$ predicted using the world average value for the tau lifetime of 303 ± 6 fs in equation (1) and assuming tau-muon universality. Using the measured branching ratio and the world average lifetime, one can estimate the ratio of the tau Fermi coupling constant to that of the muon:

$$\mathrm{G}_\tau/\mathrm{G}_\mu \;=\; 0.99 \pm 0.03\ ,$$

in very good agreement with tau-muon universality. A slightly smaller number is obtained by asuming electron-muon universality and using the muonic branching ratio to compute $\mathrm{G}_\tau/\mathrm{G}_\mu$.

The measurements of the electronic and muonic branching ratios give a value for R^τ_{had} of 3.44 ± 0.24. Using the theoretical expression for R^τ_{had} [25] we obtain

$$\alpha_s(m_\tau) = 0.26^{+0.09}_{-0.12}.$$

Using the renormalization group [26,27] this value can be extrapolated to $Q^2 = m_Z^2$, giving

$$\alpha_s(m_Z) = 0.109^{+0.012}_{-0.028},$$

in agreement with the value of $\alpha_s(m_Z) = 0.112 \pm 0.007$ obtained from an analysis of the topology of Z decays [28].

Acknowledgements

We are greatly indebted to our technical collaborators and to the funding agencies for their support in building and operating the DELPHI detector, and to the members of the CERN SL Division for the excellent performance of the LEP collider.

Table-1

	$\tau^- \to e^-\bar{\nu}_e\nu_\tau$	$\tau^- \to \mu^-\bar{\nu}_\mu\nu_\tau$	$\tau^- \to \pi^-\nu_\tau$	$\tau^- \to \rho^-\nu_\tau$
Number of Candidates	554	687	283	694
Identification Efficiency (%)	44.4 ± 1.0	59.9 ± 1.1	34.7 ± 2.0	41.2 ± 2.0
Background in Channel (%)	6.0 ± 1.1	4.4 ± 1.2	7.9 ± 3.1	16.0 ± 2.0
P_τ	-0.12 ± 0.23	-0.05 ± 0.19	-0.35 ± 0.13	-0.24 ± 0.11
Branching Ratio (%)	18.6 ± 1.0	17.4 ± 0.9	11.9 ± 1.0	22.4 ± 1.5

References

[1] A recent detailed review of tau decays can be found in the Proceedings of the Workshop on tau lepton physics, Orsay (1990); ed. M. Davier and B. Jean-Marie, Editions Frontieres (1991).

[2] B.C. Barish and R. Stroynowski, Phys. Rep. 157 (1988) 1.

[3] A very recent report on tau physics has been written by A. Pich CERN-Th.6237/91, to appear in "Heavy Flavours", ed. A.J. Buras and M. Lindner, World Scientific, 1991.

[4] M. Danilov, plenary talk at the LP-HEP91 Conference, Geneva, July 1991.

[5] The world average on the τ lifetime was reported by P. Roudeau, plenary talk at the LP-HEP91 Conference, Geneva, July 1991. Recent measurements have been published by the LEP collaborations and the CLEO collaboration.
ALEPH collaboration, CERN-PPE/92-003 (1992);
DELPHI collaboration, P. Abreu et al., Phys. Lett. B267 (1991) 422;
L3 collaboration, B. Adeva et al., Phys. Lett. B265 (1991) 45;.
OPAL collaboration, CERN-PPE/91-164 (1991);
CLEO collaboration. A.J. Weinstein in Proceeding of the American Physical Society Conference, Vancouver, August, 1991.

[6] W. Bacino et al.,(DELCO) Phys. Rev. lett. 41 (1978) 13.

[7] Y.S. Tsai, Phys. Rev. D4 (1971) 2821.

[8] A. Pich, FTUV/89-22. Contribution to the Proceedings of the "Tau-Charm Factory" workshop, SLAC, May 23-27, 1989.

[9] S. Narison and A. Pich, Phys. Lett. B211 (1988) 183.
E. Braaten, Phys. Rev. Lett. 60 (1988) 1606; Phys. Rev. D39 (1989) 1458.
E. Braaten, S. Narison and A. Pich, CERN-TH-6070/91.
S. G. Gorishny, A. L. Kataev and S. A. Larin, Phys. Lett. B259 (1991) 144.
L. R. Surguladze and M. A. Samuel, Phys. Rev. Lett. 66 (1991) 560.
W. J. Marciano and A. Sirlin, Phys. Rev. Lett. 61 (1988) 1815.
E. Braaten and C. S. Lee, Phys. Rev. D42 (1990) 388.

[10] S. Jadach et al., Z physics at LEP1, CERN 89-08, ed. G. Altarelli et al., Vol. 1 (1989).

[11] S. Jadach and Z. Was, Comp. Phys. Commun. 36 (1985) 191.

[12] F.A. Berends, W. Hollik, and R. Kleiss, Nucl. Phys. B304 (1988) 712;
M. Böhm, R. Kleiss and W. Hollik, Nucl. Phys. B304 (1988) 687.

[13] T. Sjöstrand Comp. Phys. Comm. 39 (1986) 347.

[14] F.A. Berends, P.H. Daverveldt and R. Kleiss, Phys. Lett. B148 (1984) 489, and Comp. Phys. Comm. 40 (1986) 271.

[15] DELPHI Collaboration, P.Aarnio et al., Nucl. Instr.& Meth. A303 (1991) 233.

[16] DELPHI Collaboration, P.Aarnio et al., Nucl. Phys. 367B (1991) 511.

[17] J.E. Augustin, ECFA/LEP report 29, CERN 79-01 (1979) 499.

[18] A. Rougé, Z. Phys. C48 (1990) 75.

[19] K. Hagiwara et al., Phys. Lett. B235 (1990) 198.

[20] E. Longo and I. Sestili, Nucl. Instr. and Meth. 128 (1985) 283.

[21] P. Bambade and P. Zalewski. DELPHI note 92-32, PROG-183.

[22] S. Jadach and Z. Was, "Z Physics at LEP", CERN Report 89-08 (1989) Vol. I, P 235. and CERN-TH-5994/91 (1991). T. Sjöstrand and M. Bengtsson, Comp. Phys. Comm. 43 (1987) 367, Version 7.2.

[23] ALEPH Collaboration, D. Decamp et al.,Phys.Lett. 265B (1991) 430.

[24] OPAL Collaboration, G. Alexander et al.,Phys.Lett. 266B (1991) 201.
[25] A. Pich, CERN-TH 5940/90 (1990).
[26] W.J. Marciano, Phys. Rev. D29 (1984) 580.
[27] See M. Aguilar-Benitez et al., Phys. Lett. B239 (1990) 1, and references therein.
[28] DELPHI Collaboration, CERN-PPE/91-181/Rev (1991).

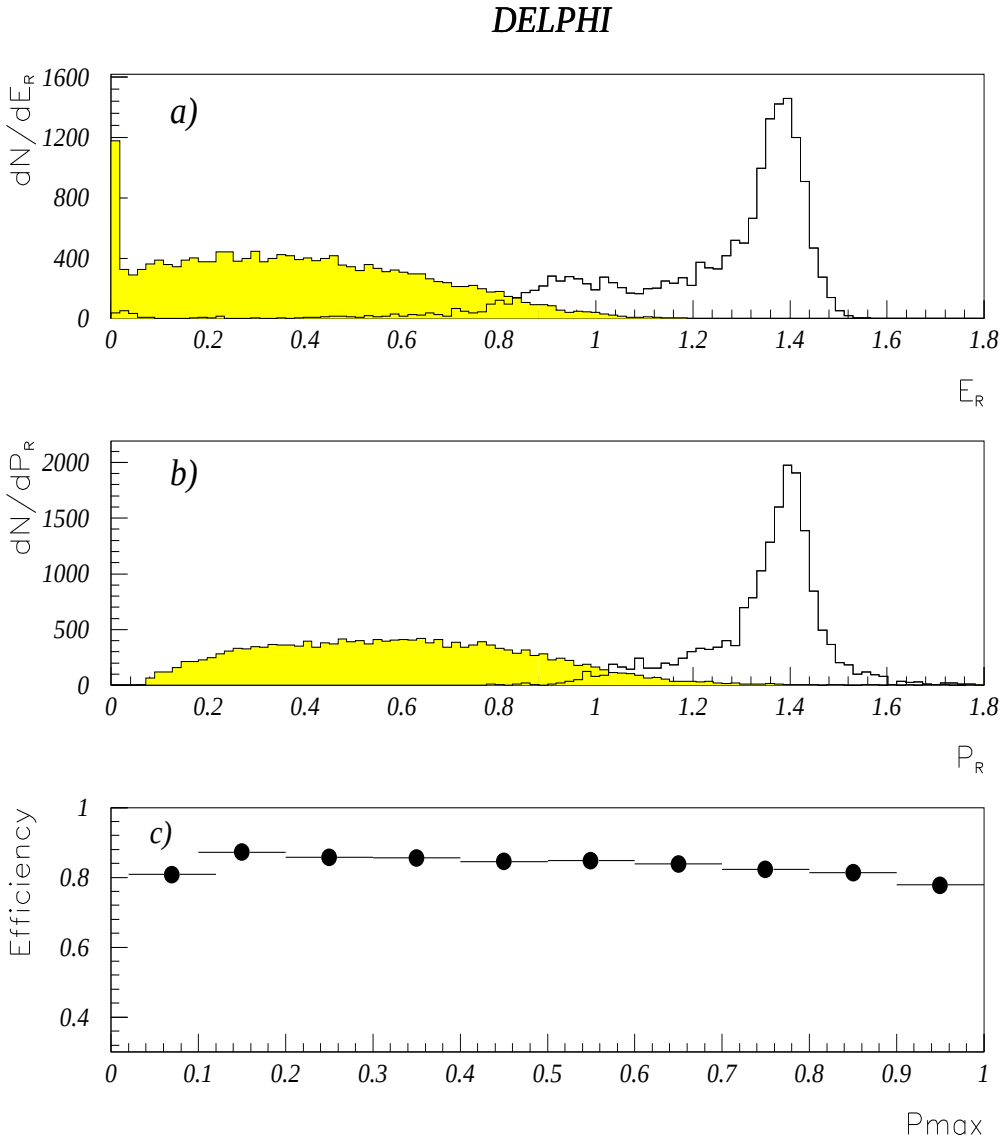

Figure 1: (a) E_R variable for Monte Carlo simulated $e^+e^- \rightarrow \tau^+\tau^-$ (shaded) and $e^+e^- \rightarrow e^+e^-$ events (expected to peak at $E_R = \sqrt{2}$) in units of E_{beam}; (b) P_R variable for Monte Carlo simulated $e^+e^- \rightarrow \tau^+\tau^-$ (shaded) and $e^+e^- \rightarrow \mu^+\mu^-$ events (expected to peak at $P_R = \sqrt{2}$)in units of E_{beam}; (c) Efficiency of the filter as a function of the momentum of the particle with maximum momentum on the event in units of E_{beam}.

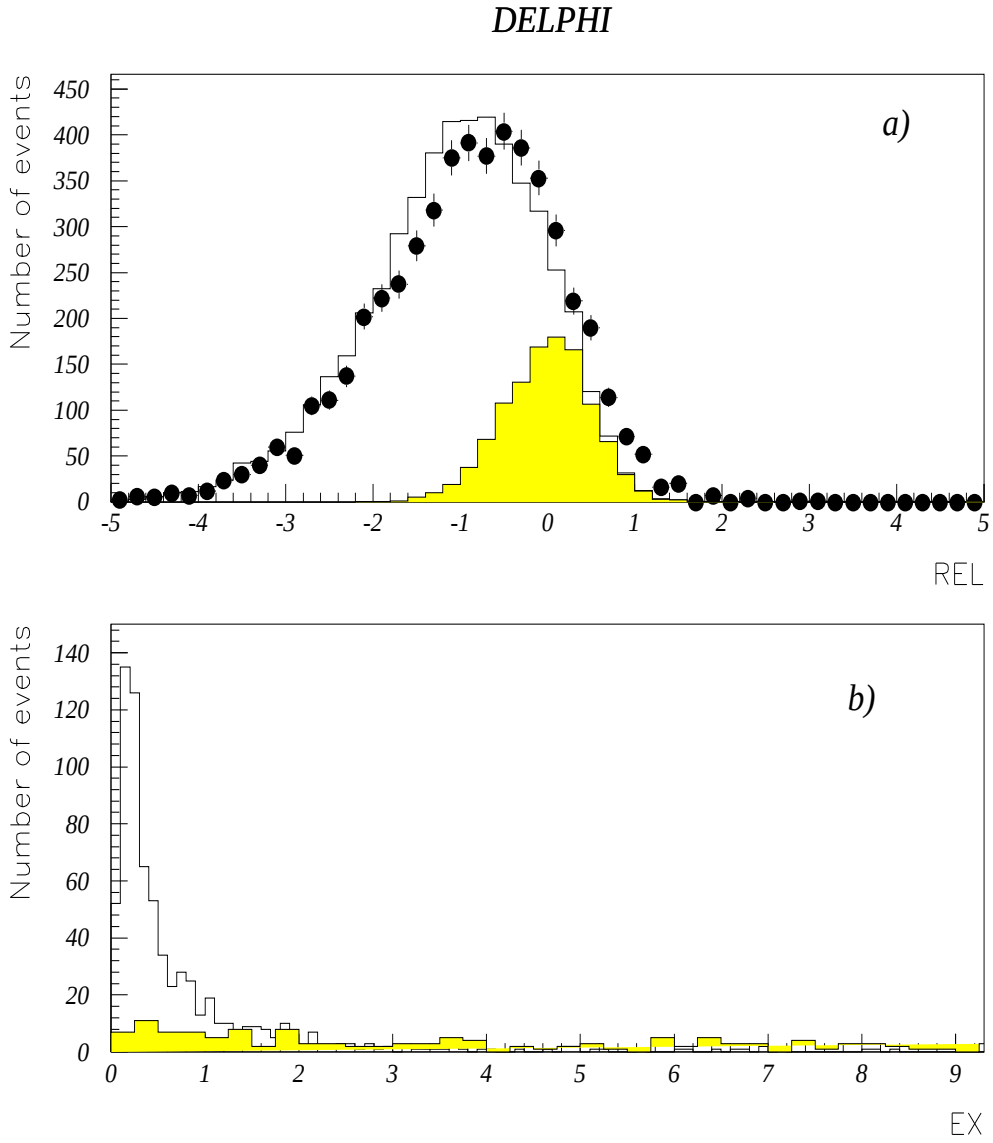

Figure 2: Variables used for electron identification. (a) REL distribution for single tracks with more than 2 GeV/c momentum (dots with error bars). Superimposed are the Monte Carlo predictions for electrons (shaded) and hadrons. (b) EX distribution for the electron and hadron (shaded) data samples. The normalisation between the two samples is arbitrary.

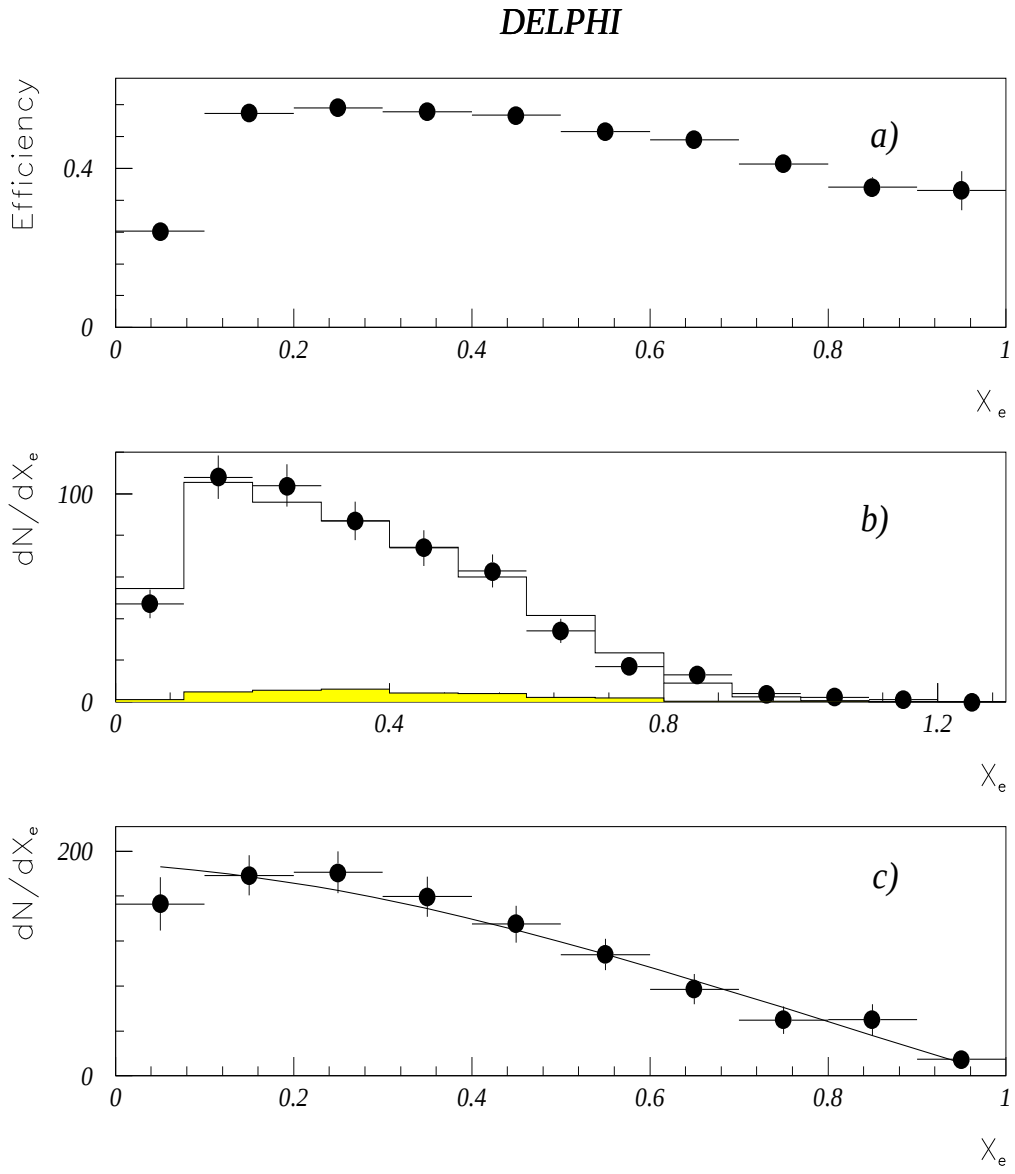

Figure 3: (a) Selection efficiency for the decay $\tau^- \to e^- \bar{\nu}_e \nu_\tau$ plotted as a function of the electron energy in units of E_{beam}. (b) Distribution of measured energy in the decay $\tau^- \to e^- \bar{\nu}_e \nu_\tau$ in units of E_{beam}. The points with error bars are the the data. Superimposed are the Monte Carlo prediction for the signal and the background (shaded). The simulated events where generated assuming the Standard Model prediction $P_\tau = -0.16$. (c) Corrected energy distribution of the decay $\tau^- \to e^- \bar{\nu}_e \nu_\tau$ in units of E_{beam}. The points with error bars are the data. The fit is superimposed.

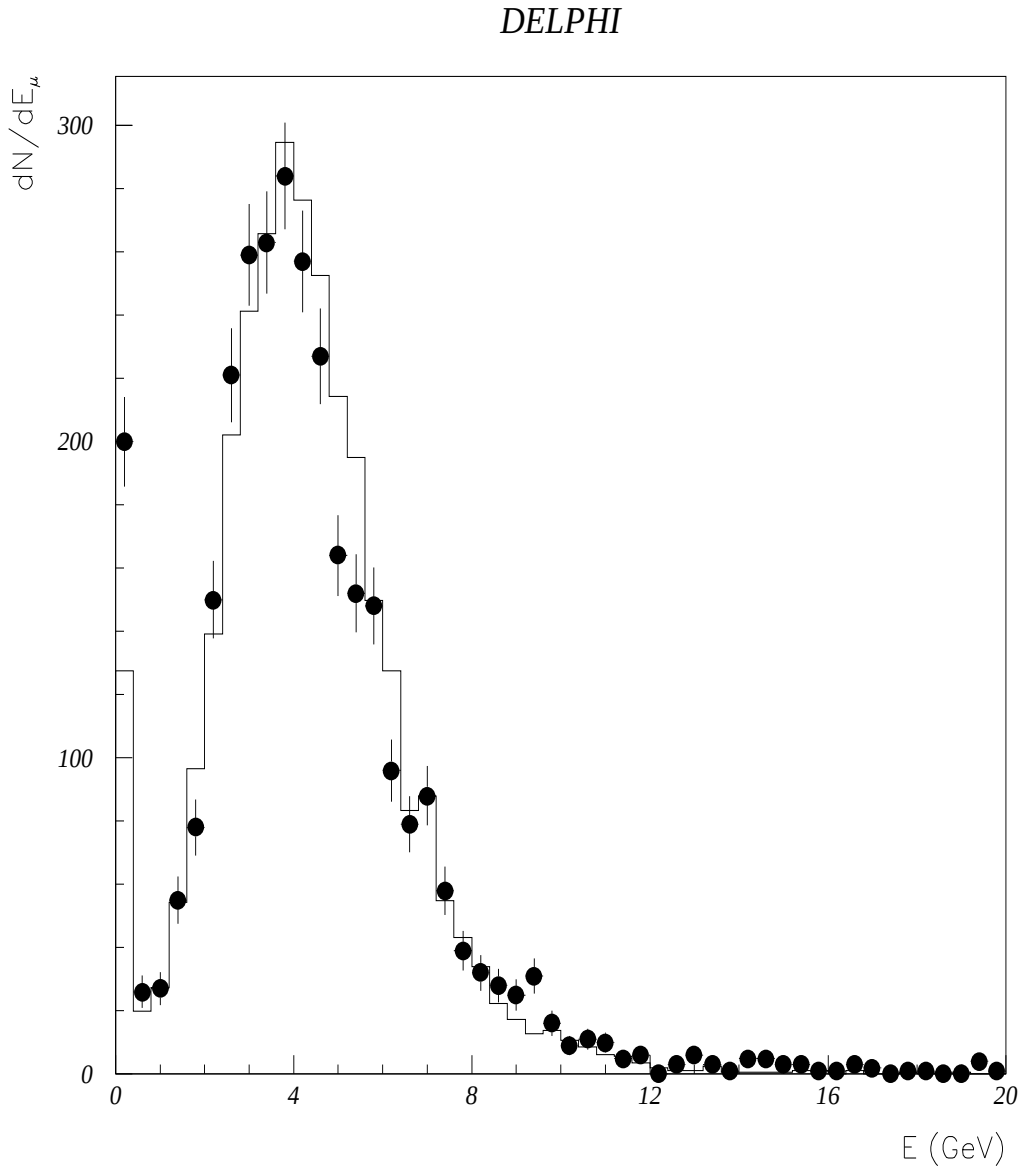

Figure 4: Energy deposition in the HCAL for muons from data (points) with Monte Carlo superimposed (solid line).

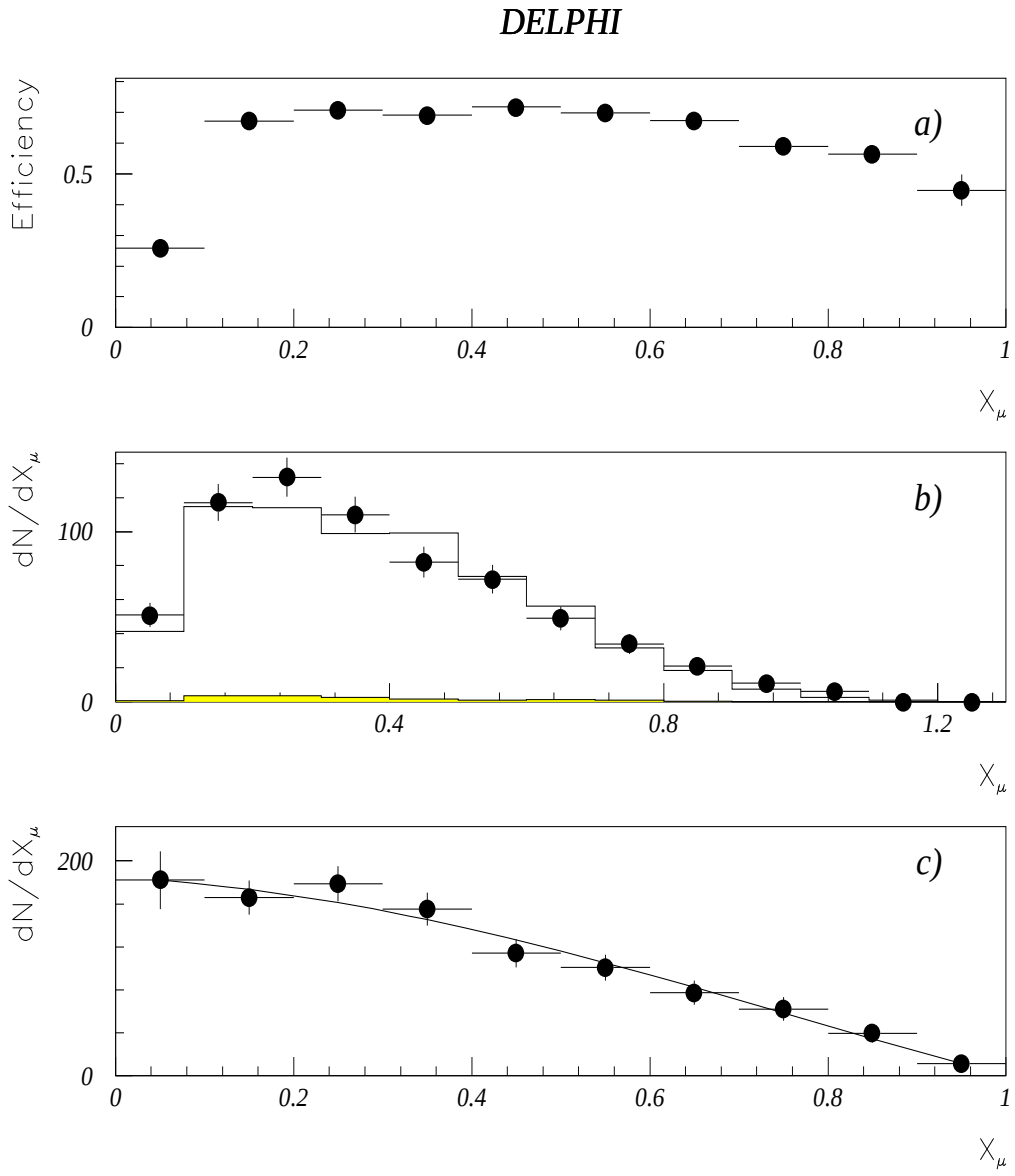

Figure 5: (a) Selection efficiency for the decay $\tau^- \rightarrow \mu^- \bar{\nu_\mu} \nu_\tau$ plotted as a function of the muon momentum in units of E_{beam}. (b) Distribution of measured momenta in the decay $\tau^- \rightarrow \mu^- \bar{\nu_\mu} \nu_\tau$ in units of E_{beam}. The points with error bars are the the data. Superimposed are the Monte Carlo prediction for the signal and the background (shaded).The simulated events where generated assuming the Standard Model prediction $P_\tau = -0.16$. (c) Corrected momentum distribution of the decay $\tau^- \rightarrow \mu^- \bar{\nu_\mu} \nu_\tau$ in units of E_{beam}. The points with error bars are the data. The fit is superimposed.

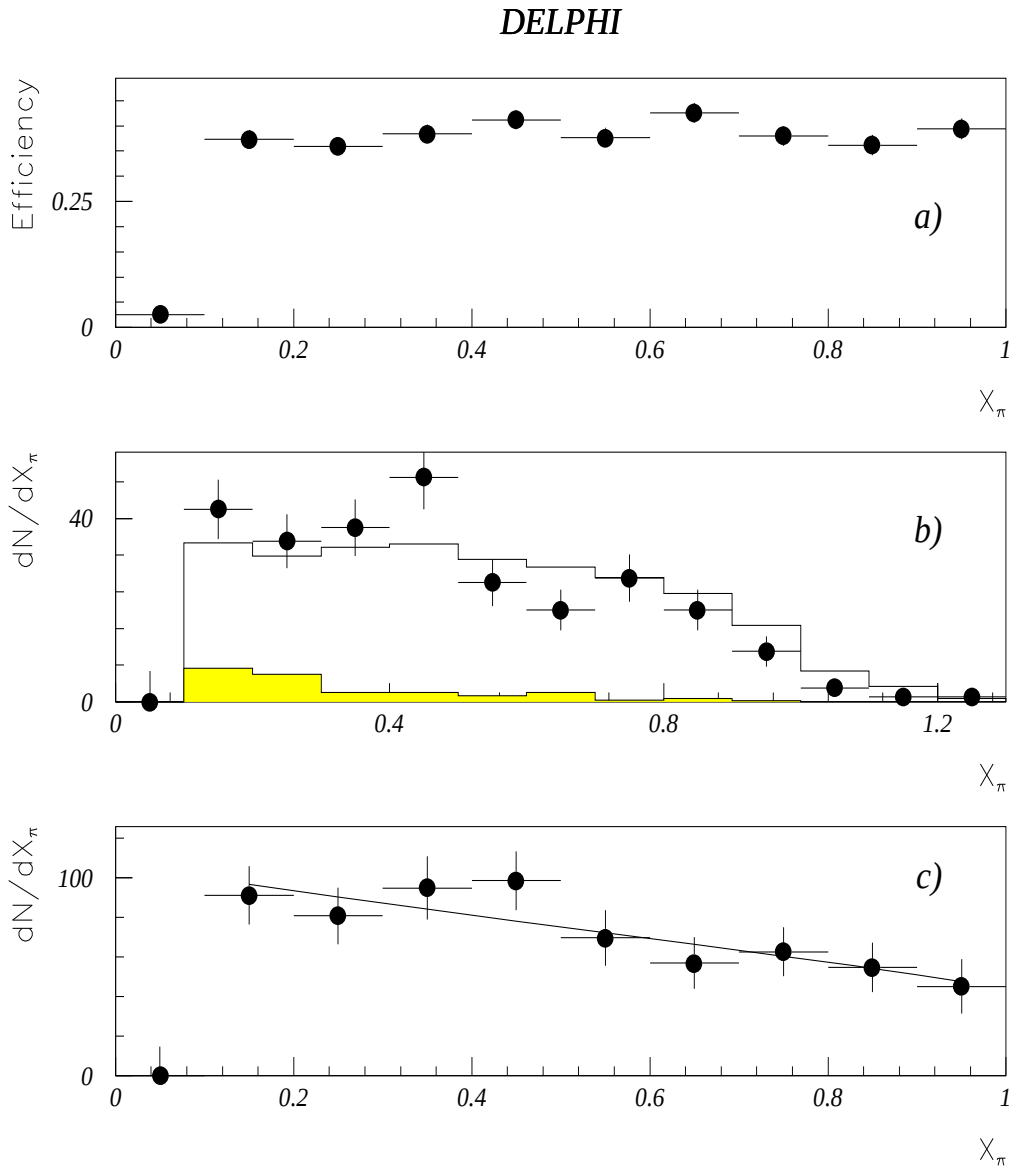

Figure 6: (a) Selection efficiency for the decay $\tau^- \to \pi^-(K^-)\nu_\tau$ plotted as a function of the pion momentum in units of E_{beam}. (b) Distribution of measured momenta in the decay $\tau^- \to \pi^-(K^-)\nu_\tau$ in units of E_{beam}. The points with error bars are the data. Superimposed are the Monte Carlo prediction for the signal and the background (shaded).The simulated events where generated assuming the Standard Model prediction $P_\tau = -0.16$. (c) Corrected momentum distribution of the decay $\tau^- \to \pi^-(K^-)\nu_\tau$ in units of E_{beam}. The points with error bars are the data. The fit is superimposed.

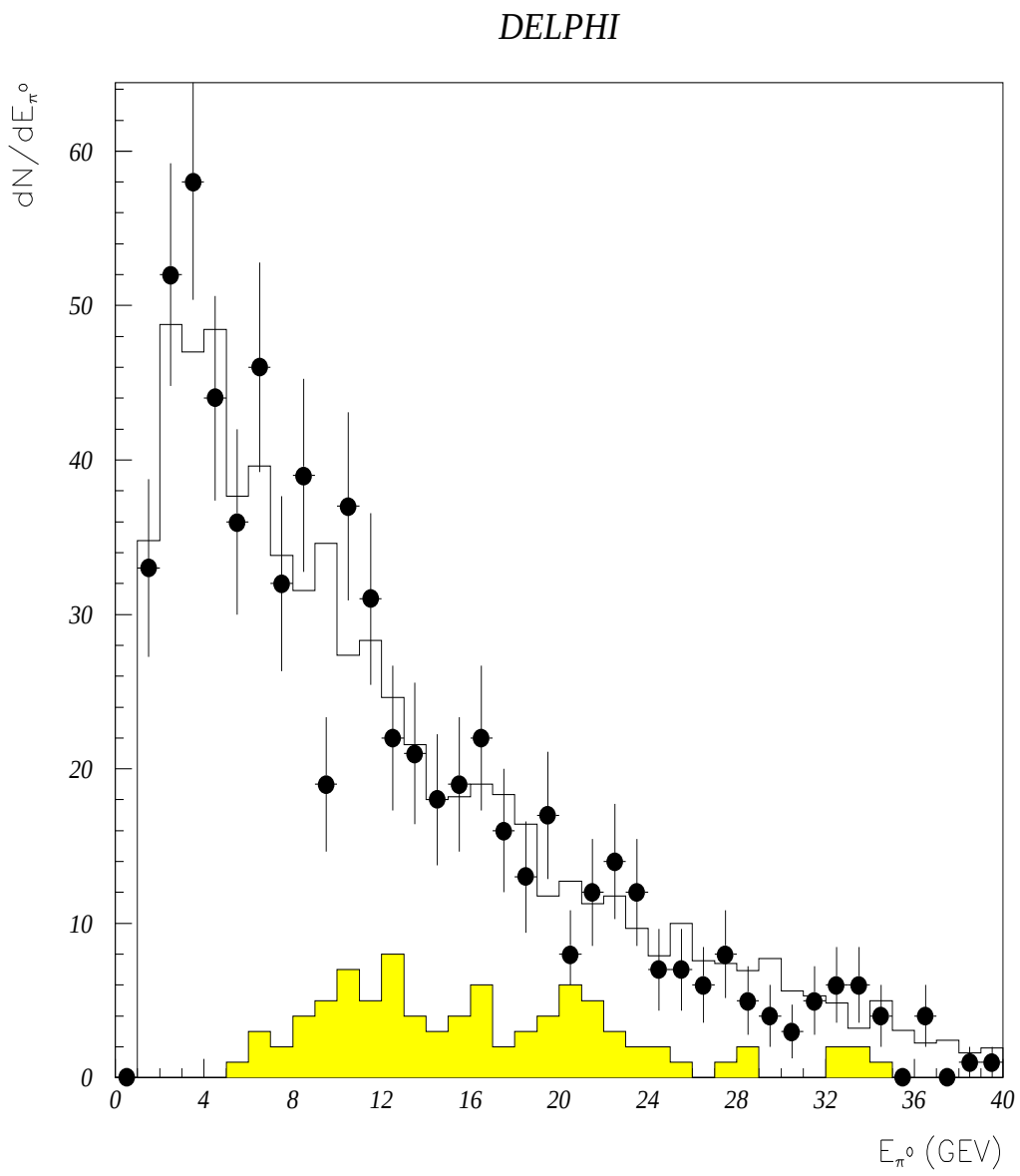

Figure 7: Energy of the neutral particle produced in the decay $\tau^- \to \rho^- \nu_\tau$, $\rho \to \pi\pi^0$; the dashed area corresponds to the contribution of the energetic π^0 (the two photons are not resolved into two neutrals but identified using the first three layers of the HPC).

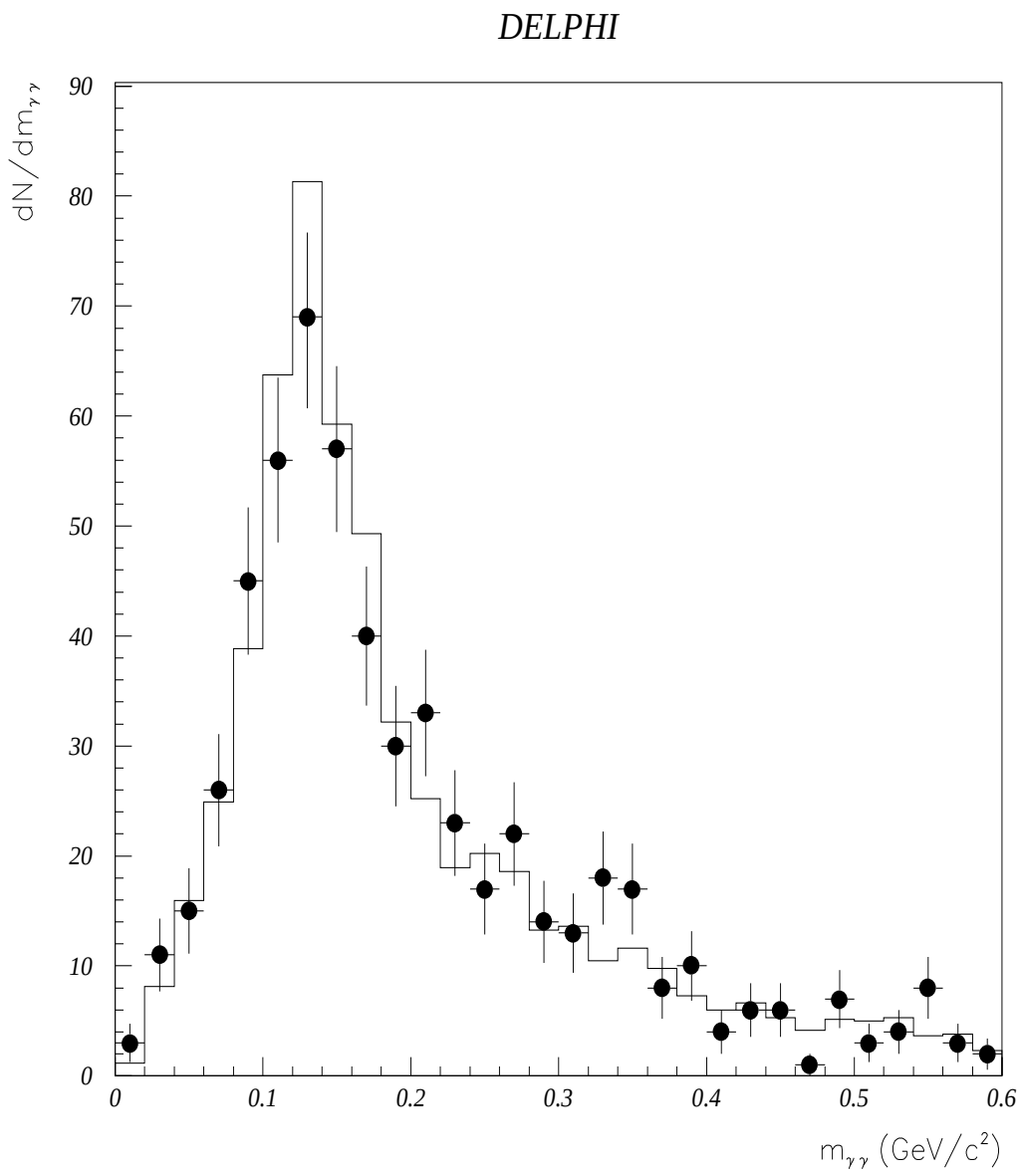

Figure 8: Invariant mass of the π^0 candidates (with the two resulting photons identified as two separate neutral particles in the HPC) for data (points with error bars) and Monte Carlo simulation (solid line).

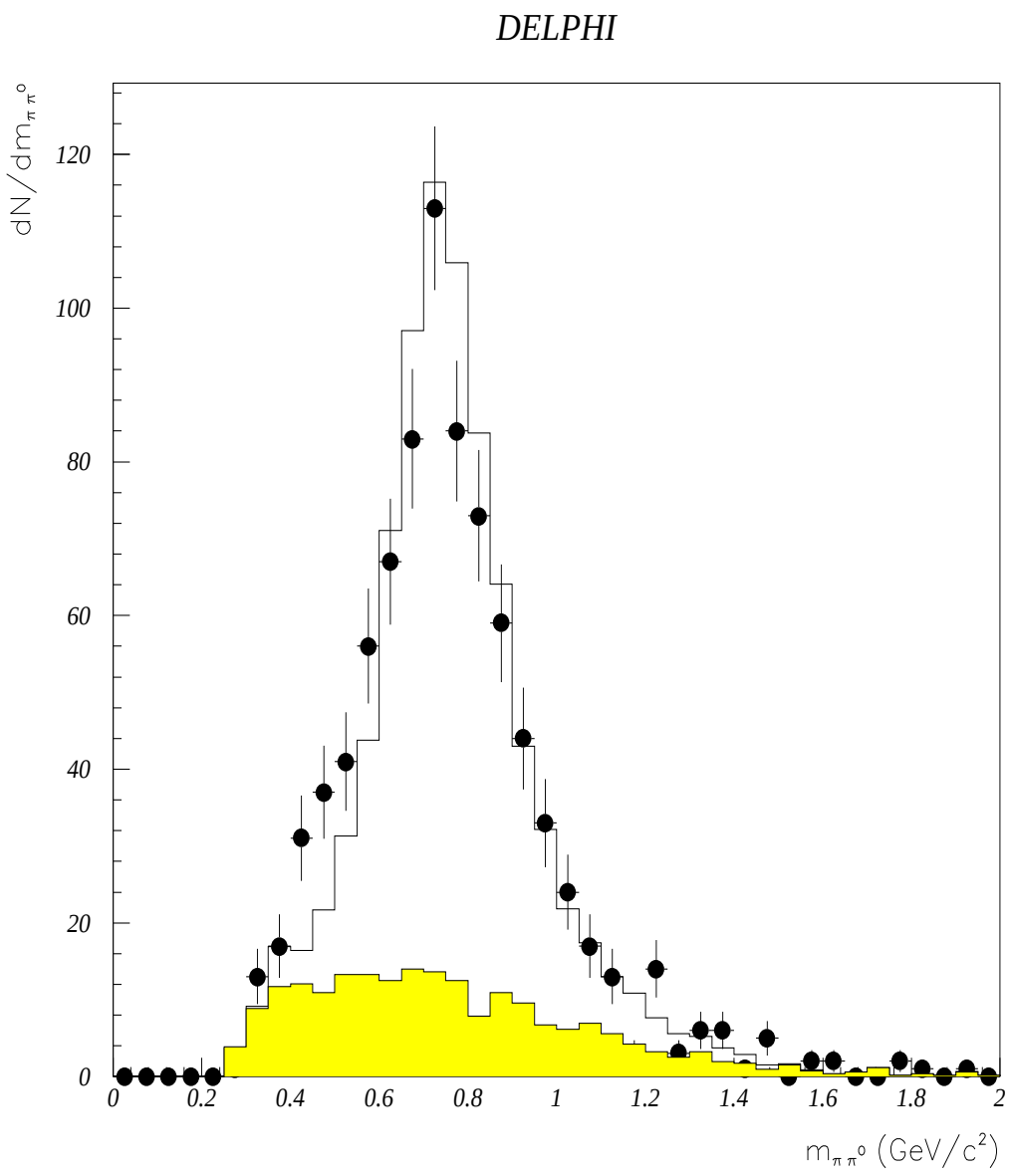

Figure 9: Invariant mass of the ρ candidates for data (points with error bars) and Monte Carlo simulation (solid line) after the cut on π^0 mass. The shaded area corresponds to the background.

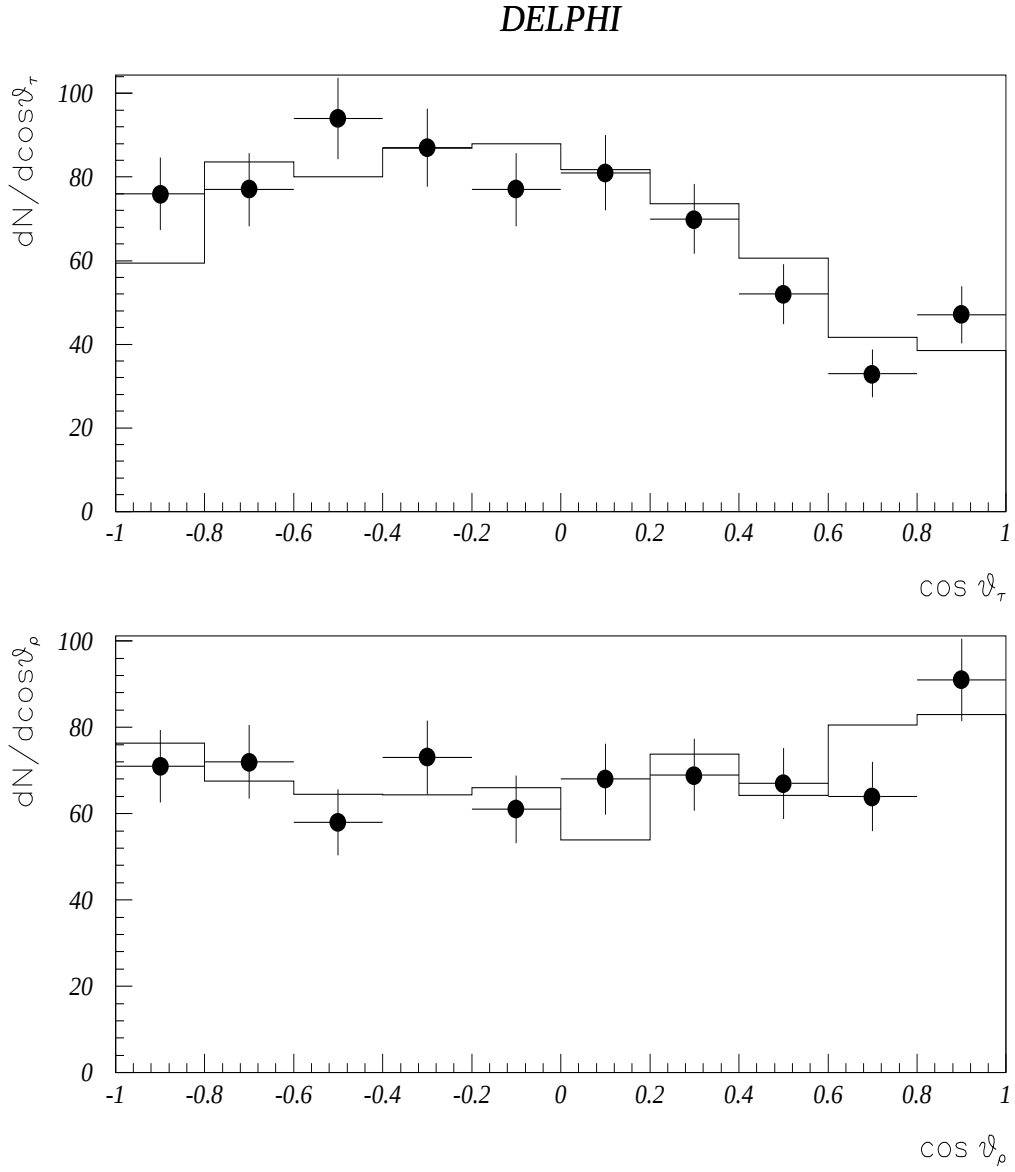

Figure 10: Raw distributions of $\cos\theta_\tau$ and $\cos\theta_\rho$ in $\tau^- \to \rho^-\nu_\tau$ events. The data are the points with error bars. The Monte Carlo prediction for $P_\tau = -0.16$ is superimposed.